IN SITV ALTERATION OF A ROCK FROM THE EARTH'S MANTLE

by

MICHAEL D. HARRELL

A THESIS

Presented to the Department of Geological Sciences
and the Honors College of the University of Oregon
in partial fulfillment of the requirements
for the degree of
Bachelor of Arts

June 1991

APPROVED: [redacted]

Dr. M. Darby Dyar

An Abstract of the Thesis of

Michael D. Harrell for the degree of Bachelor of Arts

in the Department of Geological Sciences to be taken June 1991

Title: *IN SITV* ALTERATION OF A ROCK FROM THE EARTH'S MANTLE

Approved: [redacted]

Dr. M. Darby Dyar

A composite xenolith consisting of peridotite (lherzolite) with the remnant of a pyroxenite (clinopyroxenite) dike along one side was analyzed using the technique of Mössbauer spectroscopy. This approach determines the oxidation state and crystal site distributions of the iron in each of the minerals in the pyroxenite dike (clinopyroxene and spinel) and in the peridotite (olivine, orthopyroxene, clinopyroxene, and spinel) at various distances from the pyroxenite. These data, taken together with existing microprobe analyses of the specimen, reveal certain aspects of the metasomatism of the peridotite caused by the intrusive event which emplaced the pyroxenite. Most significantly, the distribution of the iron in each of the minerals has been affected by changes in bulk chemical composition and by the substitution of divalent and trivalent cations in nearby sites.

ACKNOWLEDGMENTS

I thank Dr. Howard Wilshire of the United States Geological Survey, Menlo Park, for lending sample Ep-3-139 to me; Dr. Anne V. McGuire of the University of Houston for sending me the sample, a letter of advice on how to proceed, and unpublished microprobe data on the specimen; and Timothy S. Day and Michael B. Shaffer of the University of Oregon for assistance in the laboratory.

I thank Dr. M. Darby Dyar of the University of Oregon for serving as my thesis adviser and for providing guidance throughout this research. I thank Dr. Henry Alley of the Honors College and Dr. A. Dana Johnston of the University of Oregon for serving on my thesis committee.

I thank the National Science Foundation for supporting part of this research through the Research Experience for Undergraduates program, DMR-8900713. I thank Earle M. Chiles and the Chiles Foundation for helping me in my first four years of undergraduate study.

While I'm at it, I also thank my parents, Bruce O. Harrell and Helene C. Harrell. I certainly thank Heather M. Wilcox.

I thank you for reading this.

QVID·HOC·SIBI·VVLT

TABLE OF CONTENTS

Page

LIST OF FIGURES

Page

LIST OF TABLES

I. INTRODUCTION

Small samples of rock from as deep as 200 kilometers in the Earth's interior occasionally are brought to the surface so rapidly that they are little changed along the way. The study of such specimens provides the only direct information available on conditions deep within the upper mantle of the Earth. While the majority of these samples consist of only one rock type, some are composite, consisting of two or more types brought to the surface together, which allows the relationships between rocks coexisting at depth to be observed (Irving, 1980).

In this study, rock sample Ep-3-139 has a composite nature: the greater part of it is a common mantle rock, peridotite, which at some point was intruded by molten material. The liquid then solidified as the rock type pyroxenite, which is still present as a dike along one side of the sample. This intrusion of new material altered the original peridotite, as is seen in the darkening of the peridotite near the dike. Figure 1 gives a sketch of the specimen, and also illustrates the sections into which the sample was divided for analysis. These sections shall be referred to as Ep-3-139 A, which is the pyroxenite dike itself, and Ep-3-139 B, C, and D, the peridotite, in order of increasing distance from the dike. The analysis has focused on the iron in the minerals of each section, how it has been oxidized and how it is distributed throughout the various crystal structures, in order to see what this reveals about the process of alteration observed here, called metasomatism.

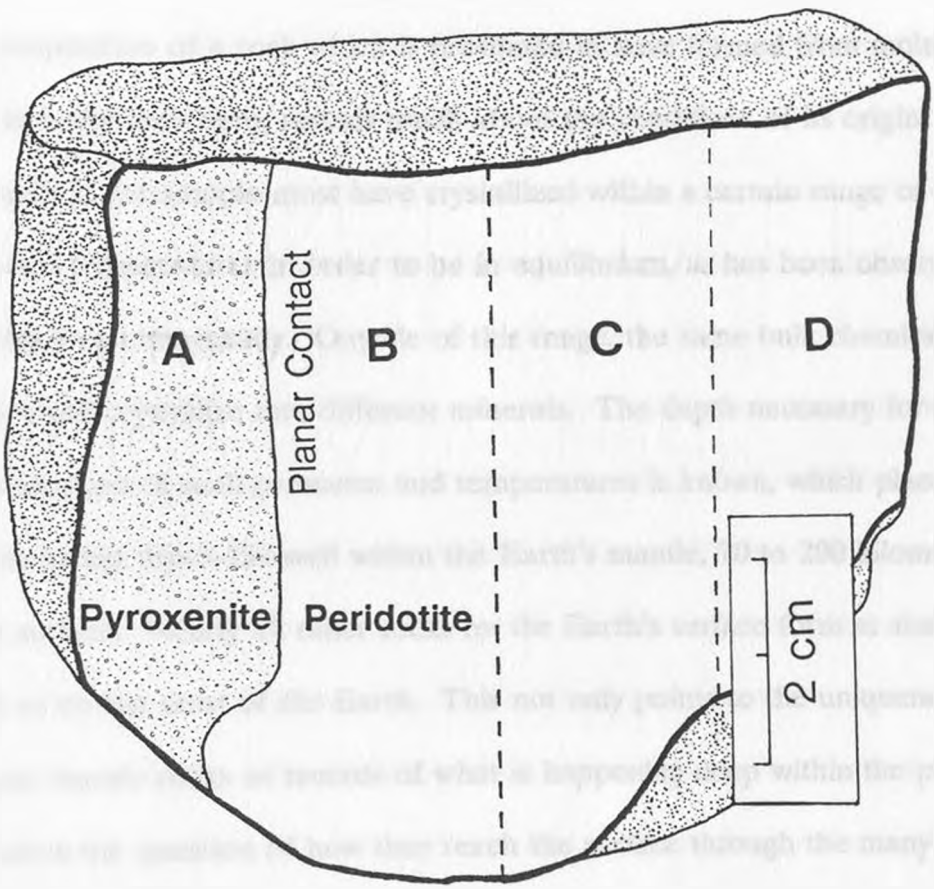

Figure 1. Perspective sketch of Ep-3-139, with front face showing the contact between the pyroxenite and peridotite, and sections A through D. The dark rind visible at the top and sides of the sample is what remains of the basalt in which the rock was encased, along with some weathering products.

II. GEOLOGIC BACKGROUND

A. Rock Origin

The composition of a rock which is presumed to have formed from molten material, as is the case here, reveals much about the conditions of its origin. The minerals seen in the sample must have crystallized within a certain range of pressures and temperatures in order to be in equilibrium, as has been observed and calibrated experimentally. Outside of this range, the same bulk chemical composition will crystallize into different minerals. The depth necessary for the natural production of such pressures and temperatures is known, which places the origin of rocks like Ep-3-139 well within the Earth's mantle, 70 to 200 kilometers below the surface. Nearly all other rocks on the Earth's surface form at shallower depths, in or on the crust of the Earth. This not only points to the uniqueness of these scarce mantle rocks as records of what is happening deep within the planet, but also raises the question of how they reach the surface through the many kilometers of overlying rock.

While the entire mechanism for transporting mantle rocks to the surface is not well understood, the environment in which these rocks are found at the surface suggest part of their history. Ep-3-139 and similar rocks occur as sparse, typically fist-sized nodules in certain lavas. Since these green inclusions appear to be so different in form and origin than the usually black volcanic basalt which encases

them, they are called 'xenoliths,' from the Greek 'foreign rock.' Xenoliths from the mantle often are present in the debris ejected from a maar, which is a rare type of volcano produced when magma from the mantle comes into contact with a source of water. The vapor produced by this contact explodes to the surface, releasing the magma, which follows at speeds estimated to be supersonic (Selby, 1985). The violence of such an event will occasionally rip pieces of adjacent rock free as the magma ascends and carry them to the surface as xenoliths embedded in the flow. The speed of transport assures that the xenoliths do not have time to react significantly with the magma which engulfs them, which accounts for the sharpness of their boundaries with the cooled basalt, and assures that they are fairly pristine samples of the mantle below (Bussod, 1983). Ep-3-139 itself comes from a maar known as Kilbourne Hole in New Mexico. Kilbourne Hole is the largest of several maars in the area, all of which are associated with the southern part of the Rio Grande rift, an area of crustal thinning and spreading which remains active to this day (Bussod, 1983). The volcanism associated with this process brought a comparative wealth of xenoliths to the surface, including Ep-3-139. The location of Kilbourne Hole is given in Figure 2.

B. Rock Composition

The two types of rock in Ep-3-139, peridotite and pyroxenite, are defined by the types of minerals present in them and the relative abundances of these minerals. In these two rock types only four minerals are present: olivine; spinel; and two pyroxenes, orthopyroxene and clinopyroxene. Peridotite contains over

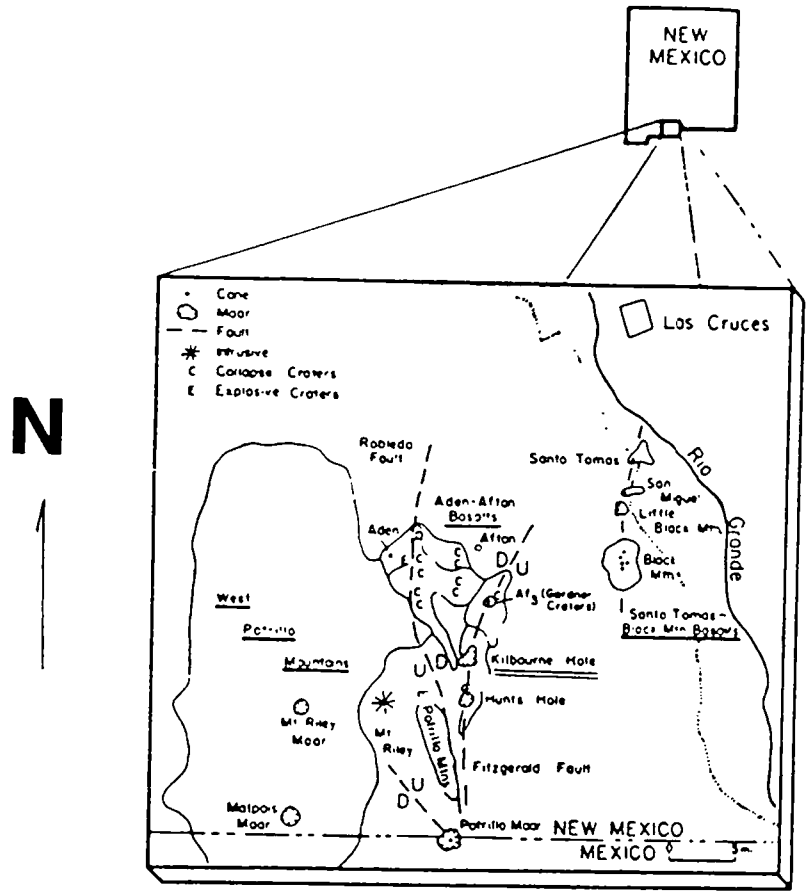

Figure 2. Location of Kilbourne Hole. Kilbourne Hole lies slightly south of center on the expanded part of the map, at 31°59'N, 106°57'W. Modified from Bussod (1980).

50% olivine, with the other minerals making up the remainder, while pyroxenite is made of more than 50% of the two types of pyroxene, with most of the rest usually being olivine (Ehlers and Blatt, 1980). In the terminology of Streckeisen (1976), the peridotite is lherzolite and the pyroxenite is clinopyroxenite; however, the terms 'peridotite' and 'pyroxenite' will be employed here. The minerals in Ep-3-139 are described in Appendix A. This appendix also sets forth the crystallographic terminology which will be used later.

The relative abundance of minerals, or the mode of Ep-3-139, was estimated from the examination of two thin sections of the rock viewed under a petrographic microscope. The pyroxenite is 80% clinopyroxene and 20% spinel. It also contains a trace amount of olivine which has been interpreted as coming from the peridotite (McGuire, 1990). The overall mode of the peridotite is 67% olivine, 18% orthopyroxene, 12% clinopyroxene, and 3% spinel, but this varies across the specimen. Near the dike, the rock is richer in clinopyroxene and spinel, up to 20% and 5% respectively, and poorer in olivine, which drops to 60%, and in orthopyroxene, which drops to 15%. In other similar composite xenoliths from Kilbourne Hole, this trend in the mode either is not present or is reversed, with spinel and clinopyroxene becoming less abundant near the dike (Irving, 1980).

C. Evidence for Alteration

Aside from the change in mode noted above, another indication that the peridotite has been metasomatized by the pyroxenite dike arises from examinations of the sample's chemical composition. This type of data supports

the view that the intruding pyroxenite changed the peridotite in a manner which can be observed to change systematically with distance from the dike within the seven centimeter width of the peridotite portion of the specimen. This forms the framework within which the present analysis of the rock will be interpreted.

As part of the overall study of sample Ep-3-139, the chemical compositions of the minerals in the sample were determined at various distances from the vein by McGuire (1991). The following description of the method employed is included because that work presently is unpublished. These analyses were done at the University of Houston on a JEOL JXA-8600 automated electron microprobe, using 15 kV acceleration voltage, 20 nA beam current, 40 second count times (20 second on Na_2O), with a beam focused to <1 μm (LaB_6 filament). The standards used were natural and synthetic minerals and glasses, with Tracor Northern ZAF matrix correction. Analytical errors are $\pm$0.2-1.0 relative percent for major elements (>5 wt%), $\pm$1-5 relative percent for minor elements (1-5 wt%), and $\pm$5-10 relative percent for trace elements (<1 wt%).

The results of these analyses, broken down by mineral type, are given in the lower halves of Tables 1 through 4. The columns headed "KH-77" represent a calculated standard xenolith which will be introduced in the Discussion section. It should be noted that the distribution of iron among its ferric (Fe^{3+} or Fe_2O_3) and ferrous (Fe^{2+} or FeO) species was done with the Mössbauer data which form the basis of this thesis, except for KH-77. The microprobe is unable to distinguish between these two types of iron. When several microprobe analyses were

Table 1. Olivine Data for Ep-3-139

	A	B	C	D	KH-77
Mössbauer Parameters					
I.S. M1		1.14	1.14	1.14	
Q.S. M1		2.88	2.89	2.90	
Width M1		0.25	0.25	0.25	
Area M1		53	54	58	
I.S. M2		1.15	1.15	1.16	
Q.S. M2		3.08	3.09	3.10	
Width M2		0.24	0.24	0.23	
Area M2		47	46	42	
%Misfit		0.00	0.01	0.00	
%Uncertainty		0.00	0.00	0.00	
Weight Percent of Oxides					
SiO2	41.01	41.97	41.82	41.73	39.75
FeO	13.37	12.06	10.37	9.50	11.41
Fe2O3	0.00	0.00	0.00	0.00	0.00
MgO	45.79	45.76	48.37	48.06	48.10
MnO	0.19	0.17	0.13	0.15	0.10
CaO	0.19	0.16	0.14	0.14	0.07
NiO	0.28	0.33	0.41	0.41	0.39
SUM	100.83	100.45	101.24	99.99	99.82
Cations Per Four Oxygens					
Si	1.012	1.031	1.014	1.020	0.986
Fe2+	0.276	0.248	0.210	0.194	0.237
Fe3+	0.000	0.000	0.000	0.000	0.000
Mg	1.685	1.676	1.748	1.751	1.778
Mn	0.004	0.004	0.003	0.003	0.002
Ca	0.005	0.004	0.004	0.004	0.002
Ni	0.006	0.007	0.008	0.008	0.008
SUM	2.988	2.970	2.987	2.980	3.013

Table 2. Orthopyroxene Data for Ep-3-139

	B	C	D	KH-77
Mössbauer Parameters				
I.S. M1	1.18	1.18	1.18	
Q.S. M1	2.42	2.42	2.40	
Width M1	0.31	0.30	0.31	
Area M1	26	25	26	
I.S. M2a	1.15	1.15	1.15	
Q.S. M2a	2.15	2.16	2.14	
Width M2a	0.27	0.27	0.28	
Area M2a	42	44	49	
I.S. M2b	1.13	1.13	1.12	
Q.S. M2b	1.87	1.87	1.85	
Width M2b	0.32	0.32	0.31	
Area M2b	23	22	17	
I.S. Fe3+	0.33	0.33	0.34	
Q.S. Fe3+	0.90	0.90	0.90	
Width Fe3+	0.49	0.49	0.48	
Area Fe3+	9	9	8	
%Misfit	0.00	0.00	0.01	
%Uncertainty	0.00	0.00	0.00	
Weight Percent of Oxides				
SiO2	53.55	54.44	54.55	54.14
Al2O3	5.27	4.70	4.31	4.27
TiO2	0.20	0.12	0.06	0.17
FeO	6.82	6.19	5.68	6.76
Fe2O3	0.75	0.68	0.55	0.48
MgO	30.80	31.51	31.95	32.18
MnO	0.16	0.14	0.15	0.15
Cr2O3	0.64	0.71	0.87	0.27
CaO	1.47	1.48	1.51	0.79
Na2O	0.10	0.10	0.11	0.09
NiO	0.10	0.16	0.11	0.15
SUM	99.86	100.23	99.85	99.45
Cations Per Six Oxygens				
Si	1.870	1.887	1.894	1.891
Al	0.217	0.192	0.176	0.176
Ti	0.005	0.003	0.002	0.004
Fe2+	0.199	0.179	0.165	0.198
Fe3+	0.020	0.018	0.014	0.013
Mg	1.603	1.629	1.654	1.676
Mn	0.005	0.004	0.004	0.004
Cr	0.018	0.019	0.024	0.007
Ca	0.055	0.055	0.056	0.030
Na	0.007	0.007	0.007	0.006
Ni	0.003	0.004	0.003	0.004
SUM	4.002	3.997	3.999	4.009

Table 3. Clinopyroxene Data for Ep-3-139

	A	B	C	D	KH-77
Mössbauer Parameters					
I.S. M1	1.19	1.19	1.19	1.18	
Q.S. M1	2.32	2.31	2.32	2.26	
Width M1	0.42	0.43	0.43	0.44	
Area M1	34	32	28	36	
I.S. M2	1.14	1.14	1.14	1.14	
Q.S. M2	1.92	1.95	1.97	1.94	
Width M2	0.41	0.40	0.40	0.40	
Area M2	38	48	52	46	
I.S. Fe3+	0.36	0.31	0.28	0.20	
Q.S. Fe3+	0.84	0.80	0.73	0.62	
Width Fe3+	0.60	0.66	0.72	0.67	
Area Fe3+	28	20	20	18	
%Misfit	0.02	-0.01	0.00	0.00	
%Uncertainty	0.01	0.00	0.00	0.00	
Weight Percent of Oxides					
SiO2	48.40	49.96	51.68	51.74	51.54
Al2O3	8.97	6.96	4.99	4.81	7.10
TiO2	1.03	0.68	0.15	0.12	0.62
FeO	4.21	3.46	2.82	2.78	2.75
Fe2O3	1.82	0.96	0.78	0.68	0.67
MgO	14.64	16.14	17.51	17.53	15.37
MnO	0.16	0.11	0.12	0.11	0.06
Cr2O3	0.02	0.81	1.24	1.29	0.61
CaO	18.56	19.06	19.50	19.55	19.75
Na2O	1.06	1.00	0.75	0.71	1.47
NiO	0.01	0.06	0.06	0.05	0.06
SUM	98.88	99.2	99.6	99.37	100.00
Cations Per Six Oxygens					
Si	1.785	1.830	1.879	1.885	1.864
Al	0.390	0.301	0.214	0.207	0.303
Ti	0.029	0.019	0.004	0.003	0.017
Fe2+	0.130	0.106	0.086	0.085	0.083
Fe3+	0.051	0.027	0.021	0.019	0.018
Mg	0.805	0.881	0.949	0.952	0.828
Mn	0.005	0.003	0.004	0.003	0.002
Cr	0.001	0.023	0.036	0.037	0.017
Ca	0.733	0.748	0.760	0.763	0.765
Na	0.076	0.071	0.053	0.050	0.103
Ni	0.000	0.002	0.002	0.001	0.002
SUM	4.005	4.011	4.008	4.005	4.002

Table 4. Spinel Data for Ep-3-139

	A	B	C	D	KH-77
Mössbauer Parameters					
I.S. vi2+	1.05	1.04	1.06	1.06	
Q.S. vi2+	1.68	1.70	1.82	1.83	
Width vi2+	0.43	0.43	0.38	0.34	
Area vi2+	30	32	23	22	
I.S. iv2+	0.74	0.73	0.78	0.79	
Q.S. iv2+	1.74	1.73	1.84	1.83	
Width iv2+	0.33	0.32	0.32	0.32	
Area iv2+	22	20	21	20	
I.S. iv2+	0.88	0.87	0.90	0.89	
Q.S. iv2+	0.92	0.93	1.03	1.02	
Width iv2+	0.32	0.29	0.38	0.37	
Area iv2+	16	14	24	22	
I.S. vi3+	0.33	0.32	0.32	0.31	
Q.S. vi3+	0.74	0.70	0.69	0.64	
Width vi3+	0.43	0.39	0.36	0.40	
Area vi3+	32	34	32	36	
%Misfit	-0.01	0.01	0.01	0.01	
%Uncertainty	0.00	0.01	0.01	0.01	
Weight Percent of Oxides					
SiO2	0.07	0.06	0.03	0.04	0.06
Al2O3	61.84	56.37	41.82	39.67	57.38
TiO2	0.40	0.42	0.20	0.17	0.14
FeO	11.63	9.52	9.44	8.93	8.88
Fe2O3	6.09	5.45	4.94	5.59	3.65
MgO	19.35	19.64	18.15	17.96	20.24
MnO	0.12	0.12	0.17	0.15	0.10
Cr2O3	0.19	8.21	25.11	27.57	9.18
NiO	0.20	0.35	0.33	0.31	0.40
SUM	99.89	100.14	100.19	100.39	100.03
Cations Per Four Oxygens					
Si	0.002	0.002	0.001	0.001	0.002
Al(tet)	0.193	0.184	0.165	0.174	0.142
Fe2+(tet)	0.059	0.044	0.077	0.071	0.066
Mg	0.740	0.761	0.746	0.743	0.780
Mn	0.003	0.003	0.004	0.004	0.002
Ni	0.004	0.007	0.007	0.007	0.008
SUM TET	1.001	1.001	1.000	1.000	1.000
Al(oct)	1.676	1.543	1.195	1.124	1.606
Ti	0.008	0.008	0.004	0.004	0.003
Fe2+(oct)	0.191	0.163	0.141	0.136	0.126
Fe3+	0.117	0.107	0.102	0.117	0.071
Cr	0.004	0.169	0.548	0.605	0.188
SUM OCT	1.996	1.990	1.990	1.986	1.994

performed within a single region, as was the case for region B in particular, these analyses were averaged by region to give the values in the tables. This approach is reasonable in light of the fairly even distribution of the original microprobe analyses within each region.

The data are first presented in the form in which they come from the microprobe, as the weight percentages of each oxide. Below this, these figures have been recalculated to give the number of cations (positively charged atoms) relative to the number of oxygen atoms in the chemical formula of each mineral: four for olivine and spinel, six for the two pyroxenes. This step compensates for the different atomic masses and oxidation states of each element, and permits the relative amount of each to be seen on an atom-by-atom basis. Although these numbers are presented with three decimal places for consistency, the uncertainties arising from the unmeasured oxygen content of the sample makes it difficult to assess their true accuracy (Dyar, 1990).

The composition of the pyroxenite, Ep-3-139 A, indicates that it falls under the classification of an Al-augite group (Group II) spinel clinopyroxenite (McGuire, 1990). The peridotite, Ep-3-139 B-D, was originally a Cr-diopside group (Group I) peridotite which has been metasomatized to an Al-augite group (Group II) peridotite (McGuire, 1990). The overall trends in the chemical composition of its minerals with distance from the pyroxenite are similar to those of other similarly metasomatized peridotites (Irving, 1980; McGuire et al., in press): all mineral phases show enrichment in Fe near the vein, the pyroxenes are

enriched in Ti and Al, with the clinopyroxene also showing Na enrichment, and the spinel is enriched in Ti and Al, but depleted in Cr near the vein. The only anomalous chemical feature is that the spinel is enriched in Mg, rather than depleted, as in samples studied earlier (McGuire et al., in press). The alteration of this sample also differs from the others in that no new hydrous mineral phases, such as amphibole, were produced in the peridotite (McGuire, 1990). This suggests that the metasomatism observed in Ep-3-139 involved a fluid containing less water than those associated with previously studied specimens.

III. METHOD

A. Overview of Method

The technique of Mössbauer spectroscopy was used in analyzing the minerals present in Ep-3-139. This method provides data on both the oxidation state of the iron, which indicates whether an individual iron atom has surrendered two or three electrons in forming bonds, and data on the iron's coordination state, which indicates how many anions (negatively charged atoms, here oxygen) surround and are bonded to a given atom of iron. From this information, the overall degree of oxidation of the iron and the distribution of the iron throughout the crystal structures of the various minerals can be deduced. This has been done for each of the divisions of Ep-3-139, and a comparison of Ep-3-139 A through D reveals the variation in patterns of oxidation and distribution of iron with respect to distance from the source of alteration. This analytical method is an application of the Mössbauer effect, a brief description of which follows. For a more complete description, see Hawthorne (1988), Dickson and Berry (1986), or Debrunner and Frauenfelder (1971).

B. The Mössbauer Effect

The Mössbauer effect concerns the properties of atoms which are emitting and absorbing gamma rays. If the nucleus of an atom is in an excited state, which is to say that it has an excess amount of energy for some reason, it may

spontaneously release energy in order to reach a more stable, lower energy state. This energy may be released in several ways, but the process of interest here is when the nucleus releases energy in the form of a high-energy photon, or gamma ray. This gamma ray is free to travel, and may encounter another nucleus where it can be absorbed, thereby raising this second nucleus to an excited state.

Since atomic nuclei can exist only at very specific, quantized energy levels, the corresponding gamma rays which are emitted also have the specific frequency associated with the energy of the transition which produced them. For absorption to take place, the energy of the incident gamma ray must also be of exactly the correct amount. These energy levels are unique for each element, so it should be possible for the atom of one element to emit a gamma ray which would then be resonantly absorbed by another atom of the same element undergoing exactly the opposite transition. However, there is a catch. In order to satisfy the law of the conservation of momentum, some of the energy involved in emitting a gamma ray must be used up in recoil, driving the nucleus in the opposite direction of the emitted ray. This decreases the energy of the gamma ray itself, so that it is no longer of the correct amount to be absorbed. Any subsequent absorption event must also involve recoil, which requires yet more of the energy of the gamma ray. In other words, the gamma ray leaves the first atom with less energy than expected, and needs even more than expected when it arrives at the second atom, so resonant absorption of this nature should never be observed. In fact it is not, but the process can be made to work if the nuclei are not free to recoil. This

restriction exists for nuclei which are bound in solids, under the right conditions.

In a solid, the recoil of an individual nucleus must be absorbed by the entire vibrating structure of atoms which make up the solid if the system is to remain in a state of internal thermal equilibrium. However, this lattice is a quantum mechanical system, so the energy which it can absorb is quantized into fixed amounts (Debrunner and Frauenfelder, 1971). If the lattice requires more energy to be excited from one vibrational state to the next than would be supplied by the recoiling nucleus, then the lattice is unlikely to accept any portion of this insufficient energy, and the nucleus will not recoil. In quantum mechanical terms, if the necessary lattice energy is E, and the recoil energy is R, then the probability that the gamma ray will be given off without recoil is given by $f = e^{-R/E}$. If R is much less than E, then f will be close to 1 in value, and nearly all of the gamma rays from such a source will be emitted with their full amount of energy (Debrunner and Frauenfelder, 1971).

The last significant feature of the Mössbauer effect is that the placement of the absorbing nucleus in a crystal structure changes more than its ability to recoil; the values of its nuclear energy levels are also affected, which changes the energy of the gamma rays which it will resonantly absorb. These changes arise from the distortion of the electromagnetic field which the nucleus in a solid experiences relative to a nucleus which is in free space. This distortion is brought about by such environmental conditions as the oxidation and coordination states of the atom in question, so that by measuring the frequencies of the gamma rays which

are absorbed, the environment in which the absorbing nucleus resides can be deduced (Hawthorne, 1988).

C. Mössbauer Spectroscopy

1. Summary of Technique

In order to determine which frequencies of gamma rays are absorbed by the atoms in a mineral, a continuous spectrum of frequencies wide enough to include all of the necessary frequencies must be passed through a pure sample of the mineral. Those rays which pass through to the other side of the sample are then collected and counted by frequency. The frequencies corresponding to absorbed rays will show lower counts than the rest. Finally, the pattern of absorbed frequencies shown in the collected spectrum may then be analyzed to determine the state or states of the atoms in the sample.

2. Gamma Ray Source

For the examination of iron, gamma rays of the appropriate frequency are generated by the radioactive decay of cobalt to iron. The isotope ^{57}Co will spontaneously decay to ^{57}Fe. This iron is in an excited state when it is formed, and will most often emit a gamma ray of energy 14.4 keV (14,400 electron-volts) in order to reach its ground state (Hawthorne, 1988). When this takes place for cobalt embedded in solid iron, the lattice energy E is approximately 0.04 eV, and the recoil energy R is approximately 0.002 eV. This places f near 0.95, so that the iron emits nearly all of these rays without loss of energy to recoil (Debrunner and Frauenfelder, 1971). Additionally, this source has a half-life of 270 days

(Hawthorne, 1988), which is short enough to assure that a small amount of it will produce a sufficient intensity of gamma radiation, yet is still long enough for the examination of a reasonable number of samples, at one every few days, before another source must be purchased.

3. Spectrometer

To produce a broad enough spectrum from this single-frequency source, the cobalt is mounted on an oscillating motor which moves it towards and away from the stationary sample. This movement introduces a Doppler shift in the frequency of the gamma radiation which is proportional to the velocity of movement. If the cobalt is moved with constant acceleration, the gamma rays will continuously sweep through a spectrum of frequencies which can be controlled by setting the oscillator as desired (Hawthorne, 1988). The equipment used consists of an Austin Science Associates (A.S.A.) S-600 Mössbauer Spectrometer Controller driving an A.S.A. K-3 Mössbauer Linear Motor. The spectra were collected and stored in a Canberra Series 35 Plus Multichannel Analyzer. A schematic illustration of the spectrometer is given in Figure 3.

4. Sample Preparation

The mineral samples themselves were prepared in the following way: First, part of each of the four regions of the rock was crushed, ground, and sieved until an accumulation of roughly sand-sized grains was obtained. This material passes through a sieve of 45 mesh (0.355 mm openings), but is stopped by one of 60 mesh (0.250 mm openings). This size was chosen because the larger grains too

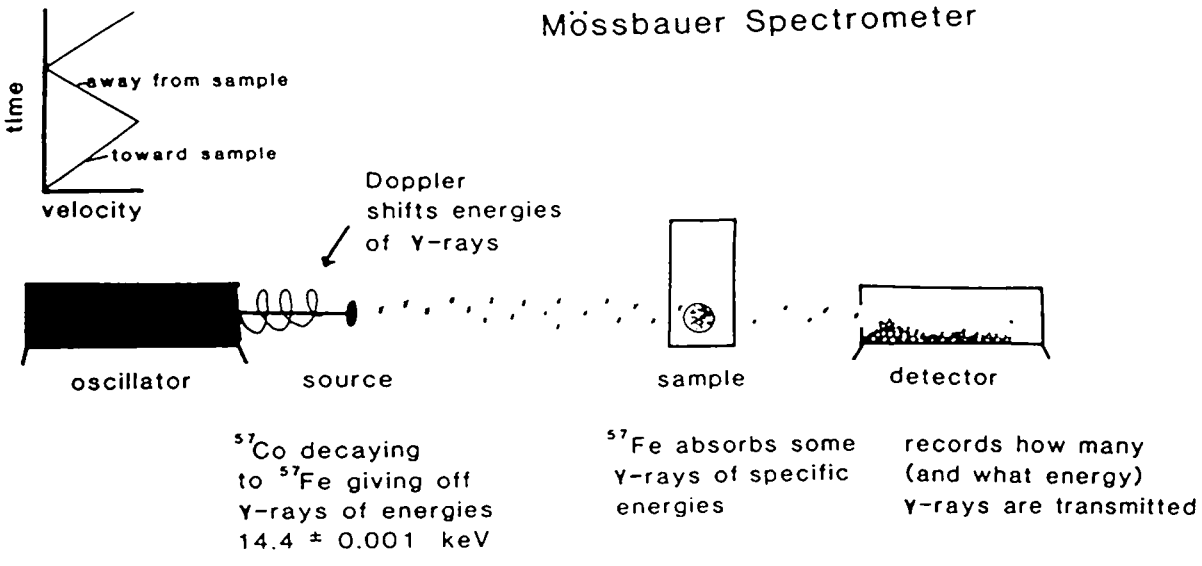

Figure 3. Mössbauer spectrometer. Used with the permission of Dr. M. Darby Dyar.

often contain more than one type of mineral in a single aggregate mass, and the smaller ones are too difficult to identify and manipulate with a brush under a 15-power microscope. Next, this material was sorted by mineral type, grain by grain, until enough of each mineral was separated for analysis. Approximately 350 mg of sample were collected for each olivine analysis, 250 mg for each pyroxene, and 100 mg for each spinel, or roughly the equivalent of a pinch of sand for each. In the case of the spinel grains, which were the most scarce and most difficult to find disaggregated, the hand-sorted separates were placed in concentrated hydrofluoric acid for two to four days. This dissolved any of the other remaining minerals but left the spinel unharmed. Next, each mineral separate was mixed with granulated sugar which was then dissolved in acetone and allowed to recrystallize as a coating on the grains, giving them a more irregular shape. This step helped to assure that the mineral grains were oriented randomly when they finally were placed in their respective plexiglass mounts, so that the gamma rays would encounter the iron in each mineral in all possible orientations.

For sample Ep-3-139, mineral separates were prepared for clinopyroxene and spinel from region A (the pyroxenite dike), and for olivine, orthopyroxene, clinopyroxene, and spinel from regions B through D, which resulted in fourteen Mössbauer spectra in all. These spectra are presented in Appendix B in their final, fitted forms. On these plots, the x-axis shows the velocity of the source relative to the stationary sample, which corresponds to the Doppler-shifted frequencies of the gamma radiation. The y-axis shows the percentage of rays of

each frequency which passed through the sample and reached the detector. A plot from a sample with no iron in it would show a straight horizontal line at the "100% Transmitted" mark.

5. Fitting

As the first step in interpreting the data, each raw spectrum was fit with a number of peaks, such that the sum of the peaks forms a curve which closely approximates the shape of the plotted data points. Each peak represents the absorption of gamma rays by iron in a particular state, and therefore each projects downward from the baseline of 100% transmission. These peaks were constrained to meet reasonable theoretical, chemical, and crystallographic criteria, in order to narrow down the infinite number of solutions which exist for any one data set, most of which have no accepted physical meaning.

Although each peak stands for iron in a unique state with its associated unique excited energy level, the peak does not occur as a spike at a single frequency, but has a definite shape and width. This is because the excited state of the iron atom decays rapidly, with a half-life on the order of 10^{-7} seconds, which makes it impossible to observe the precise energy level involved without violating the Heisenberg uncertainty principle (Hawthorne, 1988). This, combined with the exponential nature of the state's decay, the theoretical energy distribution of the emitted gamma radiation, and a consideration of the proportion of absorption events which actually produce gamma rays, leads to the selection of a Lorentzian curve for modelling each peak. For a more complete justification of this shape,

and a description of its mathematical nature, see Hawthorne (1988). For the fitting of certain materials, particularly amorphous ones such as glass, this curve is often modified by adding a Gaussian component to its shape, but this was not necessary for the spectra fit here.

The same factors which give rise to a Lorentzian curve shape for each absorption peak also limit the range of reasonable widths for such a peak, as measured at half of the peak's height. If the half-life of the excited state were too long, the peak would be too narrow to detect, while if the half-life were too short, the correspondingly wide peak would introduce too much uncertainty as to the actual nature of the energy level. The half-life of the iron transition used here produces peaks with a minimum width of 0.1940(3) mm/sec (Stevens, 1981b). In practice, if the widths fall outside of the range of 0.20 mm/sec to 0.35 mm/sec, this suggests something is wrong with the assumptions which form the basis of that particular model's fit of the data.

The entire set of peaks must also be constrained so that each peak is paired with exactly one other peak of identical width and area which differs from its partner only in position. This pair of twin peaks, known as a doublet, occurs because the excited energy level of the iron is split into two discrete levels when the atom is placed in a region where its electric field is distorted, as is the case here. Both levels of the split are equally probable for an iron nucleus in a given oxidation state and crystal site, therefore the iron atoms in each single environment produce both peaks of the doublet. This splitting of an otherwise

single state, termed quadrupole splitting (Q.S. or Δ), is shown schematically in the upper half of Figure 4. The amount of quadrupole splitting shown by each doublet is proportional to the degree of distortion of each site, and may be used to determine which doublet should be matched with any particular site, given an independent knowledge of the crystal structure and of the sites in it which are likely to be distorted to varying degrees.

Each doublet also is characterized by the displacement of its peaks along the x-axis. Again, this arises from the distortion of the nuclear energy levels in the sample relative to those of the radiation source. This is measured with respect to the zero mm/sec position, since absorption at this position would indicate that the iron in the sample is in the same type of environment as the iron in the source. This parameter, called isomer shift (I.S. or δ), is measured from zero to the midpoint of the line connecting the two peaks of the doublet, as shown in Figure 4. Typical ranges of isomer shift versus quadrupole splitting for some common minerals are shown in Figure 5.

After these parameters have been determined for each doublet in the fitted spectrum, each doublet is assigned to represent a specific crystal site containing either ferric or ferrous iron. Then the relative areas of each doublet are taken to correspond to the relative amount of iron in each site and oxidation state. This is how the distribution of ferric and ferrous iron throughout each mineral have been determined for Ep-3-139.

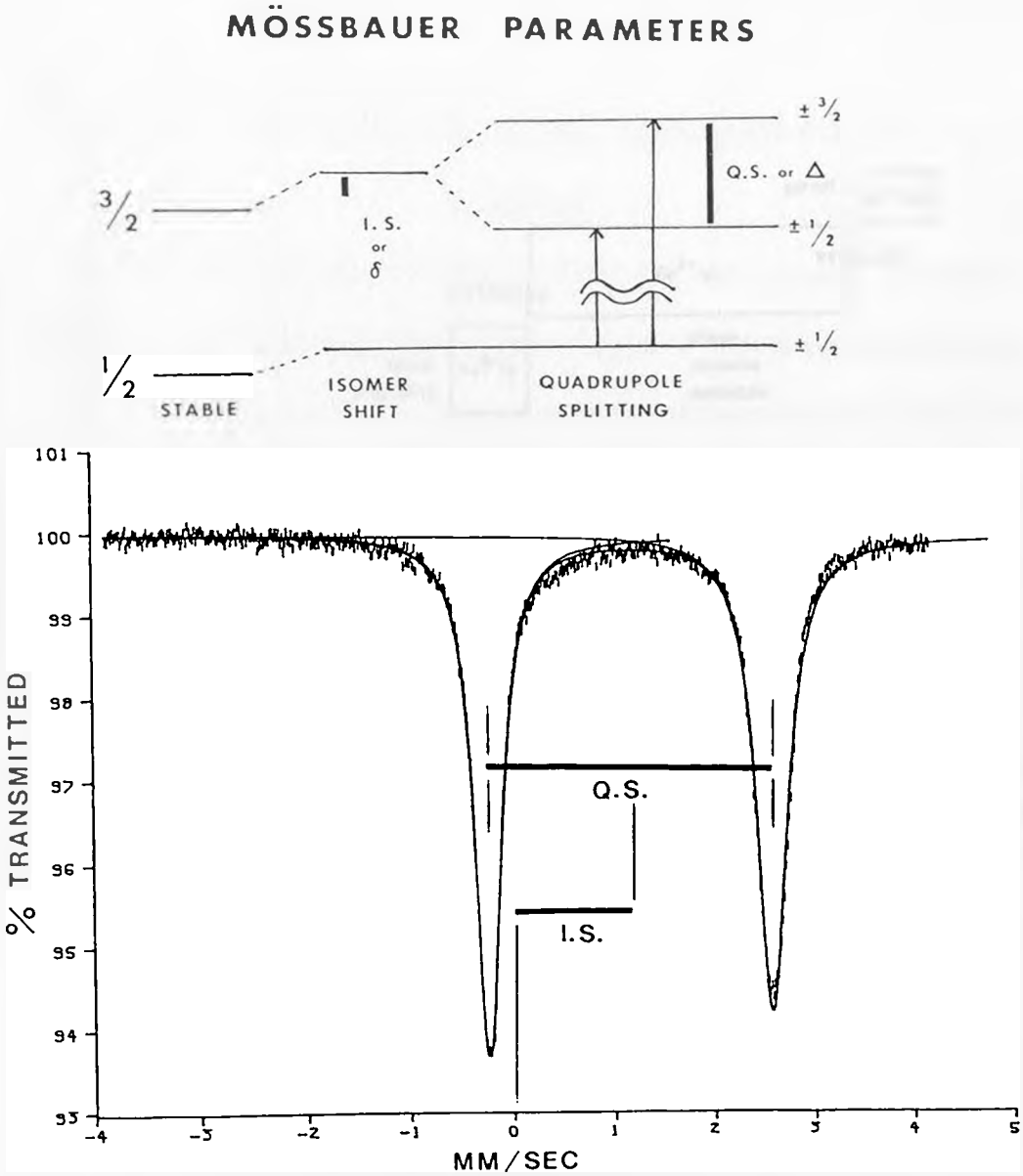

Figure 4. Mössbauer parameters for a typical spectrum. Modified from Dyar (1984).

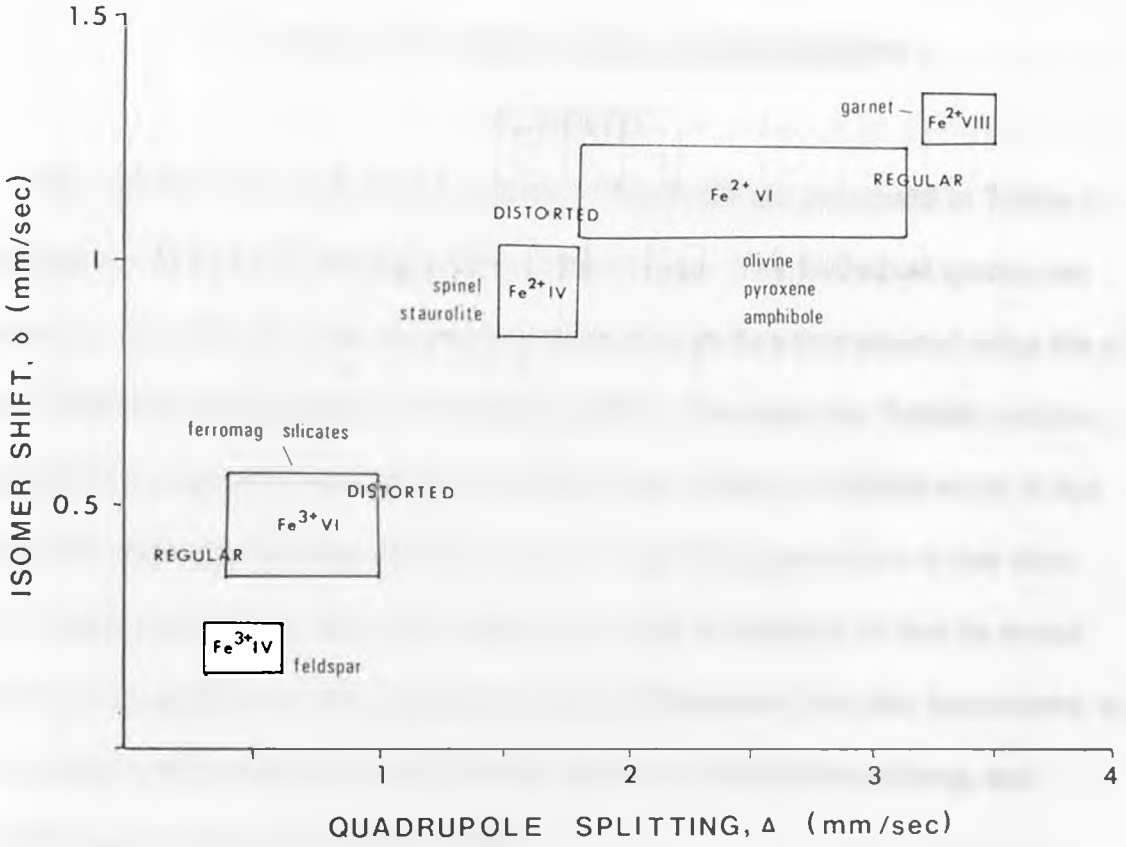

Figure 5. Isomer shift versus quadrupole splitting for some common minerals. From Dyar (1984).

IV. RESULTS, DISCUSSION, CONCLUSIONS

A. Results

The results of the Mössbauer analysis of Ep-3-139 are presented in Tables 1 through 4, where they are arranged by mineral type. The individual spectra are shown in Appendix B. The statistical quality of each fit was evaluated using the χ^2 and Misfit parameters described in Ruby (1973). The value for %Misfit and its related %Uncertainty often appears as 0.00 in the tables; a %Misfit value of less than 0.01 indicates that the statistical error of the fitting procedure is less than that which comes from the uncertainty of the data themselves, so that its actual value is not significant. The uncertainty of the Mössbauer data has been shown to be at best ±0.02 mm/sec for both isomer shift and quadrupole splitting, and ±1.5% per peak for area (Dyar, 1984).

B. Discussion

1. The KH-77 Standard

Although some variation is seen in the data from regions A through D, it is difficult to characterize what this reveals about the metasomatism of the peridotite in Ep-3-139 without reference to an unaltered standard. Bussod (1983) supplied the chemical compositions of several xenoliths from Kilbourne Hole which he believes to be unmetasomatized, most of which are very similar to one another in the composition of their minerals. However, since there is some dispute as to the

degree of local inhomogeneity of the mantle, and since it is difficult to determine which one sample best represents the original Ep-3-139 peridotite, the compositions of five of Bussod's samples (KH-77-1, -3, -6, -7, and -8, the first five in the table) were averaged together to produce the composition given as KH-77 in Tables 1 through 4. The distribution of iron between Fe^{3+} and Fe^{2+} for KH-77 was determined using average Mössbauer data calculated from another five unmetasomatized peridotite xenoliths from other maars (Dyar et al., 1989), as no such data were available for the Kilbourne Hole xenoliths. The resulting standard may contain flaws, but it does provide a point of reference from which to make some reasonable inferences.

2. Olivine

All of the iron in the olivine was determined to be Fe^{2+}. The presence of Fe^{3+} in olivine has been documented in samples from metasomatized xenoliths elsewhere, but it is still not certain whether such iron is contained within defects and distorted sites in the olivine itself, or whether it is seen because of the presence of microscopic intergrowths of other minerals within the olivine, such as laihunite ($Fe^{2+}Fe^{3+}(SiO_4)_2$) (Hawthorne, 1988; McGuire et al., in press). The fact that the Ep-3-139 olivine does not contain Fe^{3+} implies that its metasomatism is significantly different from those previously studied by McGuire and coworkers.

The distribution of Fe^{2+} between M1 and M2 sites favors the less-distorted M1 site, particularly in C and D. This preferential ordering of the iron decreases near the vein. Near the vein the total amount of Fe also increases inversely to

decreasing Mg content, as shown in Figure 6, suggesting an exchange of Fe^{2+} for Mg^{2+}. It appears that this influx of iron was unable to order itself as well as the original Fe was ordered prior to metasomatism before such cation movement became kinetically inhibited. One note of caution in this interpretation is that the change in M1/M2 distribution occurs very near the limits of resolution of the data. The total amounts of Fe and Mg remain near the values for KH-77 across the pyroxenite.

3. Orthopyroxene

The ratio of Fe^{3+} to Fe^{2+} in the orthopyroxene remains constant across the peridotite, despite the fact that the total amount of Fe increases near the vein. The only resolvable difference in the spectra is a decrease in ordering near the vein, in this case between the M2a and M2b sites. These two sites differ from one another only when a trivalent cation such as Fe^{3+} or Al^{3+} substitutes into an M1 site normally occupied by a divalent cation. Those M2 sites bordering such a distorted M1 site become M2b sites, while those bordering an undistorted M1 site are M2a sites (Dyar et al., 1989). Since the total amounts of trivalent cations such as Al^{3+} and Fe^{3+} increase as the amounts of some divalent cations (Mg^{2+} in particular) decrease, the substitution of these trivalent cations into M1 sites may account for the creation of more M2a distorted sites. The trends of these elements and their relationship to KH-77 may be seen in Figure 7.

4. Clinopyroxene

The relative amount of Fe^{3+} in the clinopyroxene is significantly greater in the

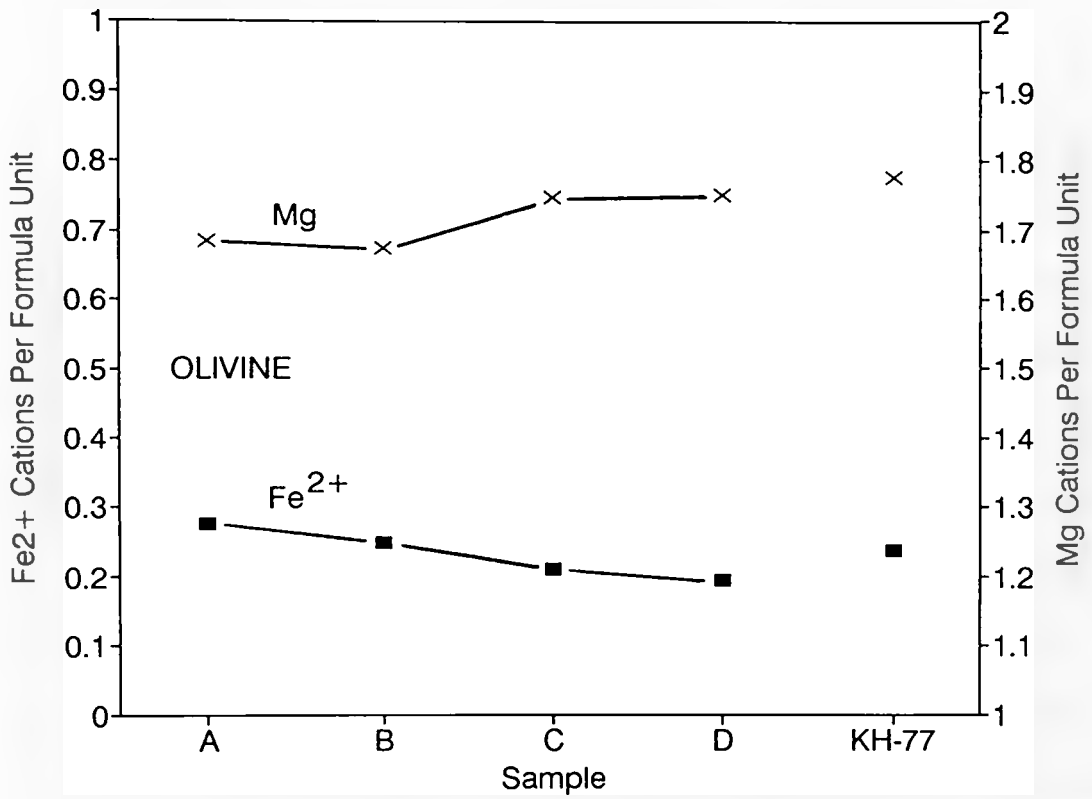

Figure 6. Plot of selected olivine data. Fe^{2+} and Mg are plotted against separate vertical axes with the same scale.

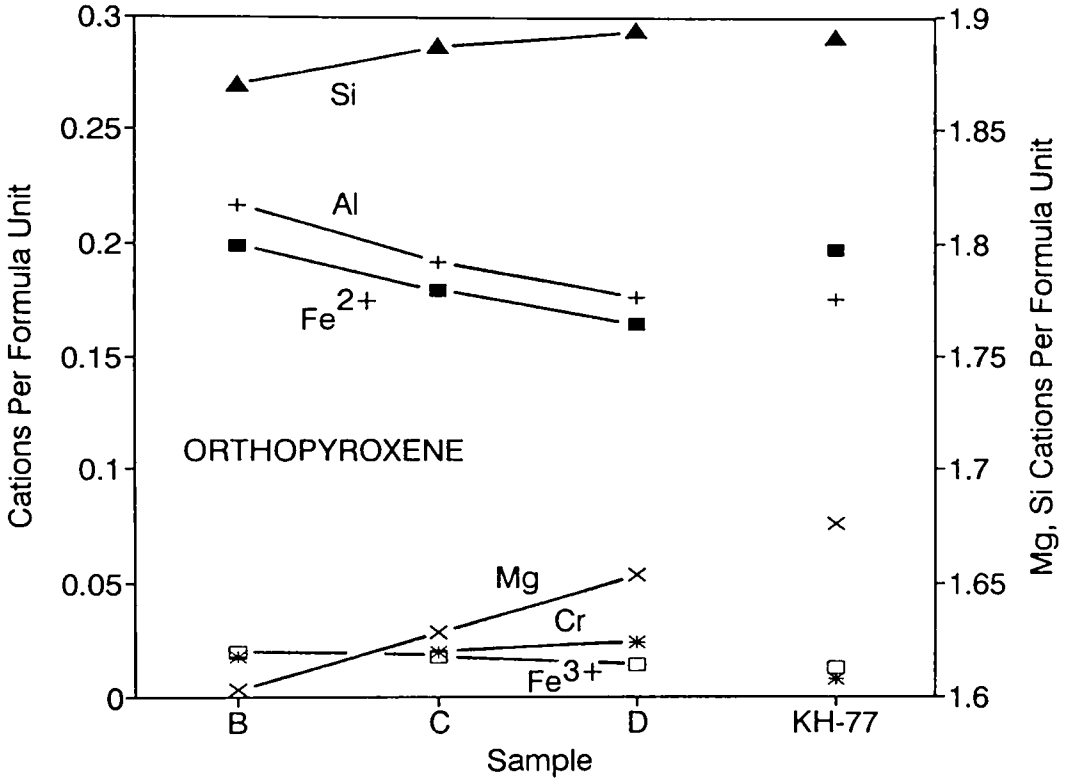

Figure 7. Plot of selected orthopyroxene data. Mg and Si are plotted against a second vertical axis with the same scale as the first.

clinopyroxenite than the peridotite (28% of the total Fe versus 20%). Within the peridotite, the ratio of Fe^{3+} to Fe^{2+} remains constant as it does in orthopyroxene, again despite the increase in total Fe near the vein. No trend in the ordering of the Fe is apparent.

As shown in Figure 8, the amounts of Fe^{3+} and Fe^{2+} are elevated above the values for KH-77 near the vein, and approach them with greater distance from the vein. While this increase in Fe content is significant (0.008 cations per formula unit for Fe^{3+}, 0.021 cations per formula unit for Fe^{2+}), the greater part of the substitution seems to have involved Al, Mg, and Si. The amount of Al increases by 0.094 cations per formula unit from Ep-3-139 D to B while the amount of Mg decreases by 0.071 cations per formula unit and Si decreases by 0.055 cations per formula unit. None of the other cations experience so great a change. As Al is substituted for Mg near the dike, the net charge balance of the clinopyroxene appears to be maintained by the substitution of Al for Si in the silica tetrahedra, along with Na substituting for Ca. As was shown by Skogby and coworkers (1990), however, clinopyroxenes which display this enrichment in Al and Fe^{3+} can contain unusually large amounts of hydrogen, which would also serve to maintain charge balance. The presence of such hydrogen would be obscured by the recalculated figures shown in Tables 1 through 4, as these are based on the assumption of stoichiometric charge balance with twelve oxygens and no hydrogen. Since no new hydrous minerals were produced by the metasomatism of this peridotite, the existence of hydrogen in the clinopyroxene, and perhaps its enrichment near the

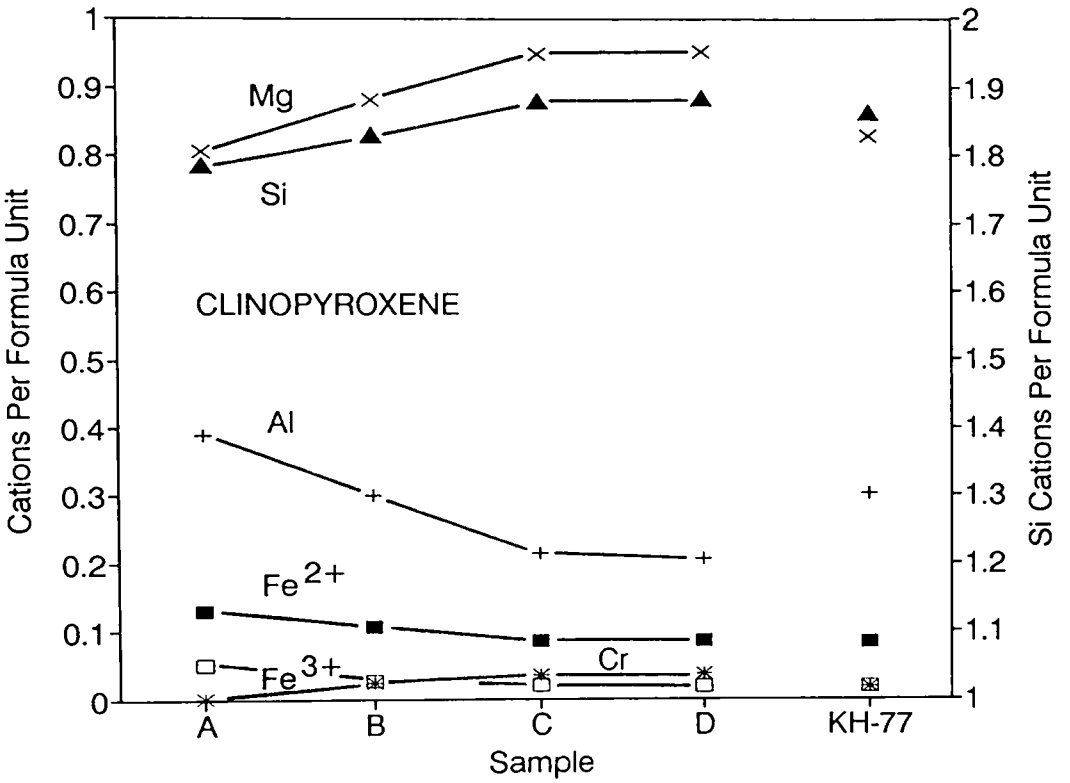

Figure 8. Plot of selected clinopyroxene data. Si is plotted against a separate vertical axis with the same scale as the first.

vein, would be significant in determining how much water was present when this alteration occurred. This question is of greatest interest in the case of the clinopyroxenite, since its clinopyroxene shows these compositional trends to the greatest extreme, and since clinopyroxene makes up the bulk of the rock.

5. Spinel

In the spinel, the ratio of Fe^{3+} to Fe^{2+} does not change significantly across the peridotite, nor does the total amount of Fe. However, the amount of Fe^{2+} in tetrahedral coordination decreases near the vein, while that in octahedral coordination increases. This is shown in Figure 9. This may be in part a response to the substitution of octahedral Al for octahedral Cr observed near the dike. While this trend in the Al follows that seen in the clinopyroxene, the odd feature of this substitution is that both the Al and Cr are near the KH-77 values at the dike, and then both diverge from this standard with distance from the dike. Although the KH-77 values conform with those of Ep-3-139 D elsewhere, these discrepancies suggest that it may not accurately represent this type of unmetasomatized peridotite in its entirety. It also may be that not all of the features observed in Ep-3-139 are the product of a single metasomatic event.

C. Conclusions

The analysis of Ep-3-139 by Mössbauer spectroscopy has revealed several characteristics of the metasomatism recorded by the sample, particularly when the results of this research are combined with data obtained by microprobe analysis of the same rock. The olivine is seen to lack Fe^{3+}, which marks a difference

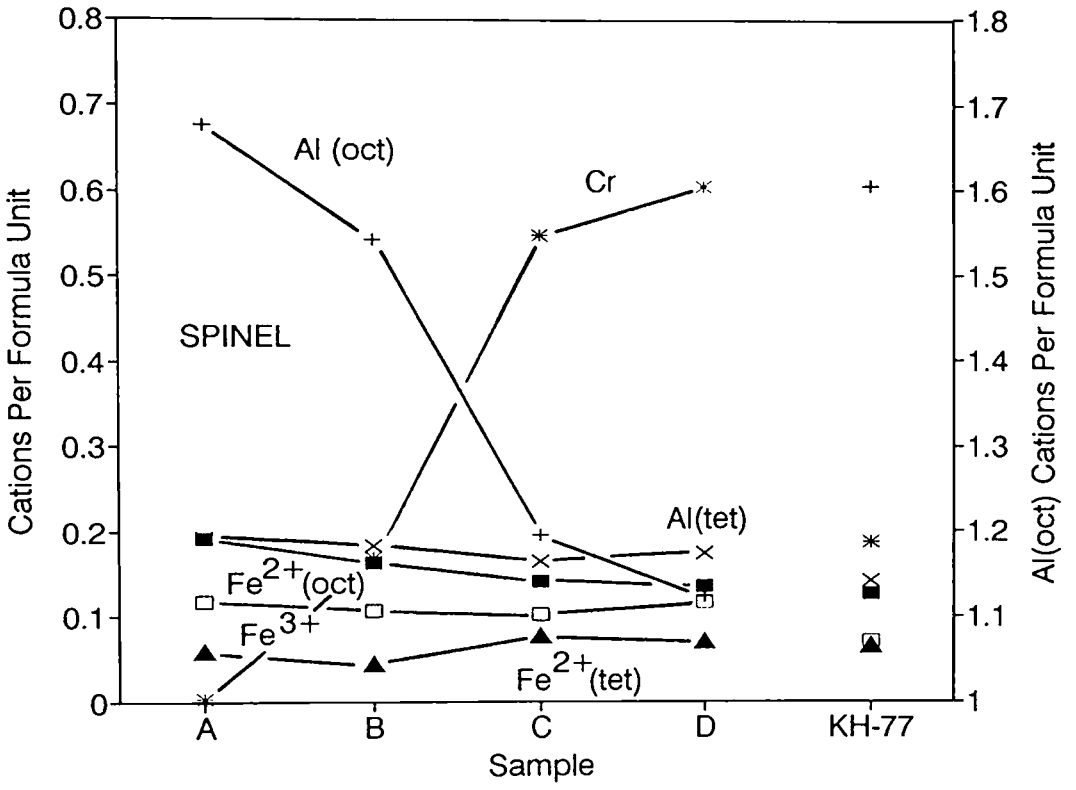

Figure 9. Plot of selected spinel data. Al(oct) is plotted against a second vertical axis with the same scale as the first.

between the alteration seen here and that of other peridotites, but there is a suggestion of greater disorder of Fe distribution near the vein, as has been observed elsewhere. The orthopyroxene also shows disordering near the vein which may be caused by the substitution of trivalent cations into sites normally occupied by divalent species. In the clinopyroxene, the increase of Fe^{3+} and Fe^{2+} points to a set of substitutions which may accommodate previously unsuspected hydrogen in the sample, and in the spinel the change in Fe^{2+} ordering may be an indication of the redistribution of Al as it substitutes for Cr.

APPENDIX A

MINERALOGY

Most minerals have a range of possible chemical compositions associated with them, because some positions in their crystal structure can be occupied by atoms of different elements, depending upon what is available at the time of crystallization. For this reason, a mineral name more often refers to a specific crystal structure and an associated spectrum of allowed compositions, rather than to a unique chemical formula. Occasionally, however, names are assigned to specific chemical compositions as well.

The mineral olivine can have the composition Mg_2SiO_4, called forsterite, or Fe_2SiO_4, known as fayalite. These two, however, are only the two ends of a continuous range of compositions with varying Mg/Fe^{2+} ratios, such as $Mg_{0.5}Fe_{1.5}SiO_4$. In this example, Mg is present as 0.5 cations per formula unit, and Fe as 1.5 cations per formula unit. The iron in olivine is normally ferrous, or Fe^{2+}, indicating that each Fe atom has given up two electrons in order to form bonds, but ferric iron, Fe^{3+}, occurs in some specimens. Other elements, such as calcium, manganese, and nickel also can substitute for magnesium or iron. The crystal structure of olivine is illustrated and interpreted in Figure 10.

The pyroxenes have a wider range of composition, and are divided into two groups, orthopyroxenes and clinopyroxenes, which have slightly different crystal

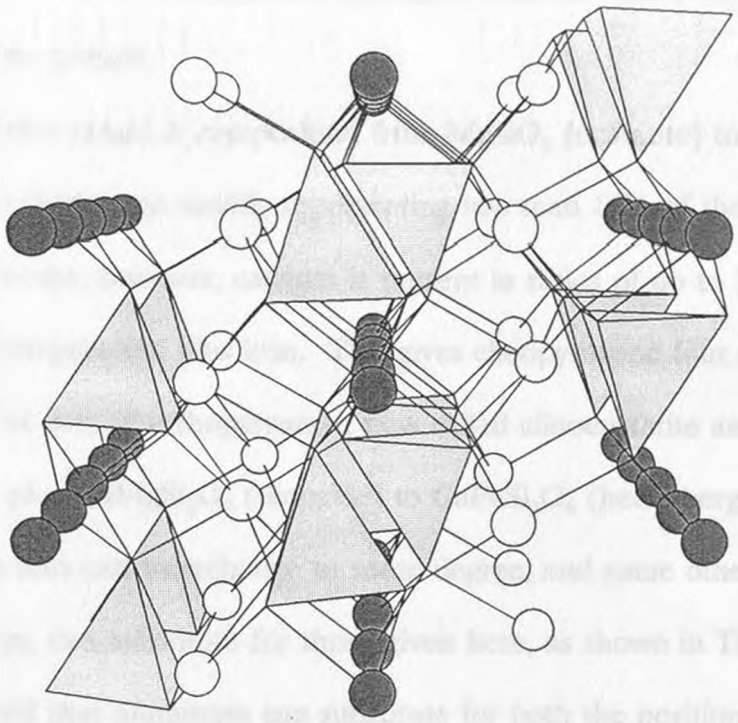

Figure 10. Crystal structure of olivine. In this schematic depiction, each tetrahedron represents five atoms: one silicon atom at the center surrounded by four oxygen atoms, one at each corner. This unit, SiO_4, is known as a silica tetrahedron. The spheres show the locations of the other individual atoms, such as iron or magnesium. Each of these is bonded to the six nearest oxygen atoms, as the connecting lines indicate. The shading of the spheres denotes the different types of positions in the structure. The dark spheres are M1 sites, which share six of these oxygens with neighboring sites, while the light M2 sites share only three oxygens, and are half a numerous. This illustration was generated by the computer program ATOMS (Dowty, 1989).

structures. Figure 11 shows a representative pyroxene, and notes the difference between these two groups.

Orthopyroxenes range in composition from $MgSiO_3$ (enstatite) to $FeSiO_3$ (ferrosilite), with ferric iron usually representing less than 10% of the total iron. In the clinopyroxenes, however, calcium is present in ratios of up to 1:1 with the total amount of magnesium plus iron. This gives clinopyroxene four end member compositions: the two of orthopyroxene, now called clinoenstatite and clinoferrosilite, plus $CaMgSi_2O_6$ (diopside) to $CaFeSi_2O_6$ (hedenbergite). Ferric and ferrous iron also can interchange to some degree, and some other elements, notably aluminum, can substitute for those given here, as shown in Tables 2 and 3. It should be noted that aluminum can substitute for both the position of magnesium and iron and the position of silicon, and that sodium interchanges with calcium.

The name spinel covers an unusually broad group of at least thirteen end member component minerals in which fifteen or more elements and both ferric and ferrous iron can substitute for X and Y in the formula XY_2O_4 in specific combinations. The spinel structure is given in Figure 12. In the spinel of Ep-3-139, the X position contains iron, manganese, magnesium, nickel, and silicon, while the Y position contains aluminum, chromium, iron, and titanium (McGuire, 1991).

The mineral data in this appendix are taken from Deer et al. (1985).

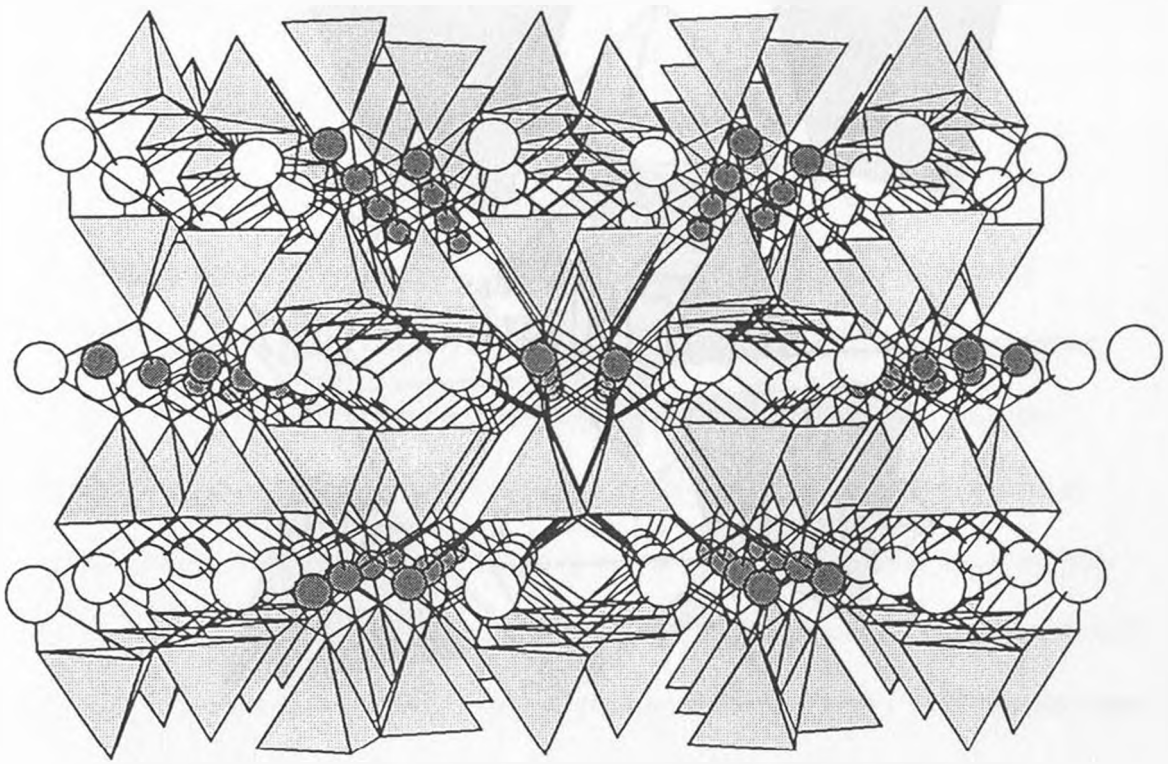

Figure 11. Crystal structure of pyroxene. As in olivine, the tetrahedra represent SiO_4, although in this arrangement each tetrahedron shares two of its oxygens with neighboring tetrahedra where their points touch, so that the ratio of silicon to oxygen is actually 1:3. The tetrahedra thus form chains of silica which are shown coming out of the illustration above, with five chains in each of the four layers of silica. Note that the apices of these chains alternate in direction. The dark M1 sites lie between apices of tetrahedra, while the light, larger M2 sites are between the faces. If both the M1 and M2 sites are occupied by small atoms, such as iron and magnesium, the silica chains fit next to each other side-by-side, forming orthopyroxene. If the M2 sites contain the larger calcium atoms, however, the structure is distorted so that the chains are offset, forming clinopyroxene. Clinopyroxene is shown above. This illustration was generated by the computer program ATOMS (Dowty, 1989).

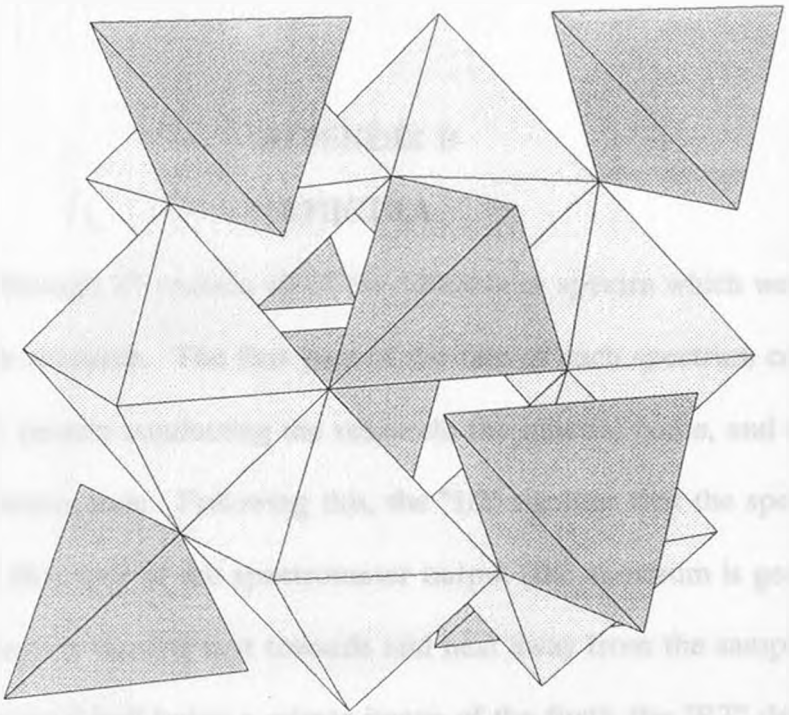

Figure 12. Crystal structure of spinel. No individual atoms are shown here. Instead, the dark tetrahedra represent one central positively charged atom, or cation, surrounded by four oxygens, and the light octahedra have one central cation surrounded by eight oxygens. Oxygens are shared wherever the points of either type of polyhedra touch. The atoms at the center of tetrahedra are said to be in four-fold coordination, and typically have given up two electrons, while those in octahedra are in six-fold coordination, and have given up three electrons. This illustration was generated by the computer program ATOMS (Dowty, 1989).

APPENDIX B

SPECTRA

Figures 13 through 25 contain all of the Mössbauer spectra which were generated in this research. The first part of the title of each spectrum contains the name of the person conducting the research, the mineral name, and the sample identification code. Following this, the "1/2" signifies that the spectrum comes from the first half of the spectrometer output (the spectrum is generated twice as the source is moving first towards and next away from the sample on each pass, with the second half being a mirror image of the first); the "RT" denotes that the sample was run at room temperature (the positions of the peaks are temperature-dependent, and much of the overlap seen here might have been eliminated if a suitable apparatus for controlling temperature were available); and the date indicates when the sample was removed from the spectrometer (the length of runs varies from a few hours to a few days, depending on the abundance of the sample and its iron content). The last two entries refer to computer data files. The first is the name under which the raw data is stored, and the second is that of the file containing the fitted data. In this second name, the fourth character is a single digit standing for the number of peaks in the fit, and the last two characters are the number of constraints used in controlling the fit.

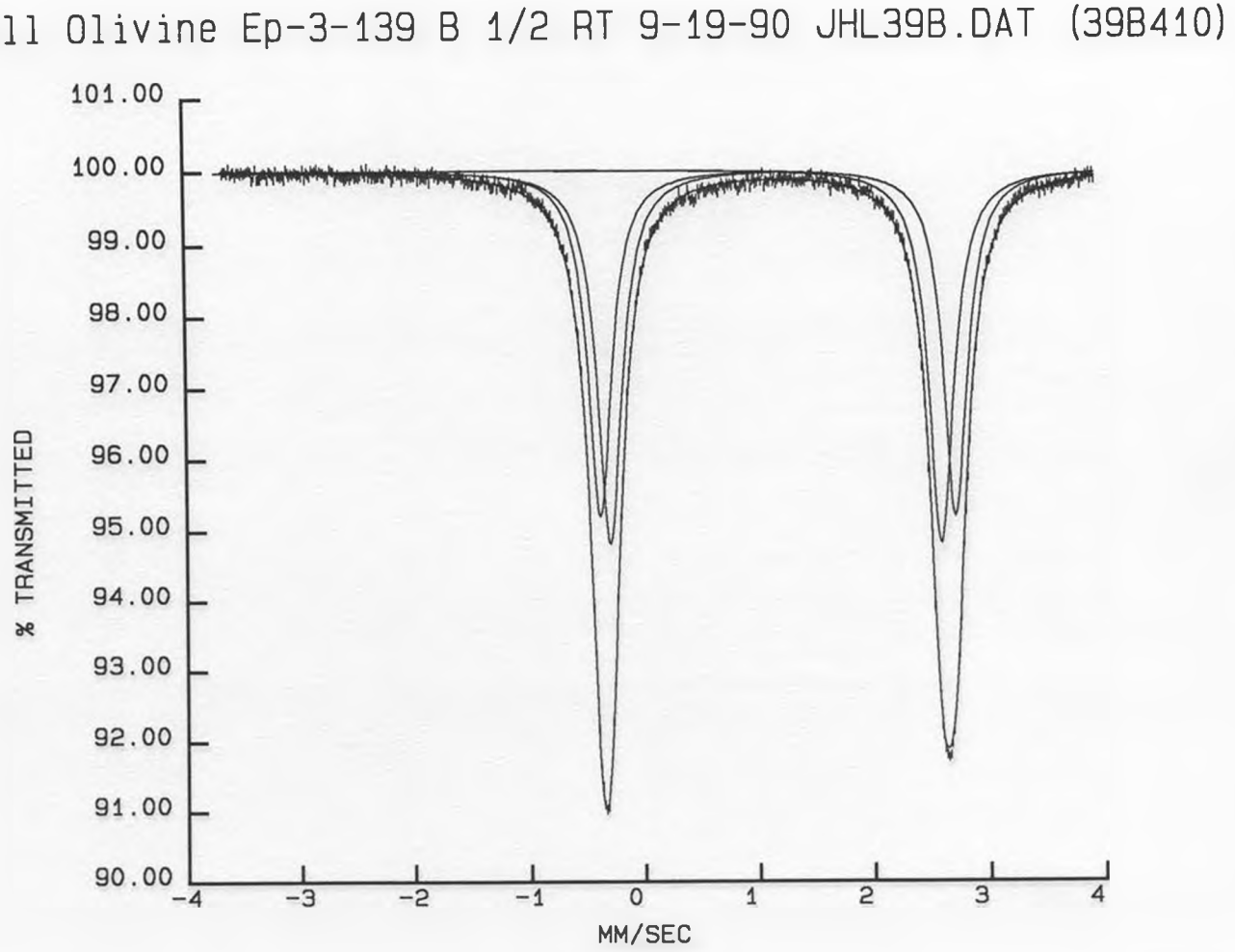

Figure 13. Mössbauer spectrum of olivine in Ep-3-139 B.

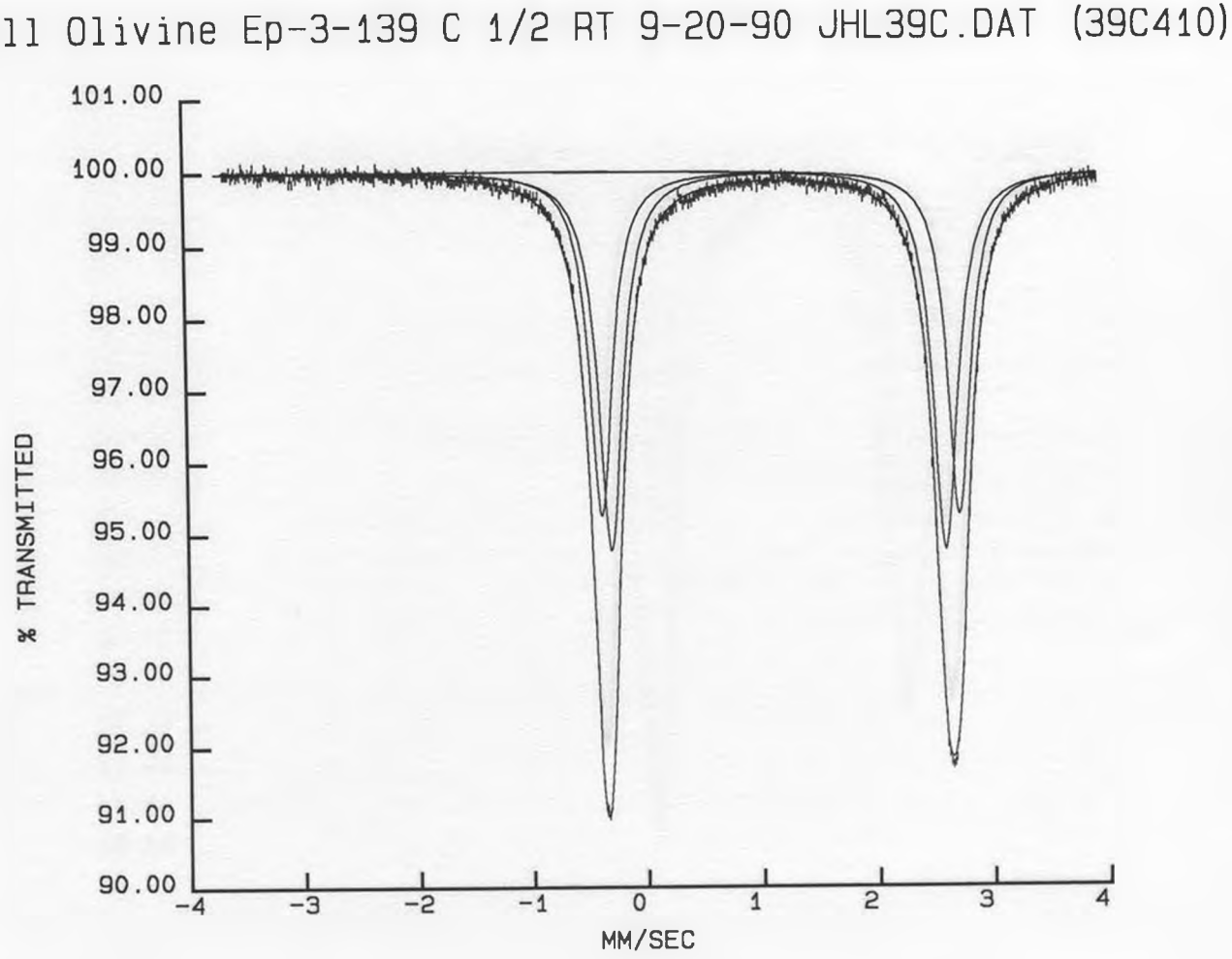

Figure 14. Mössbauer spectrum of olivine in Ep-3-139 C.

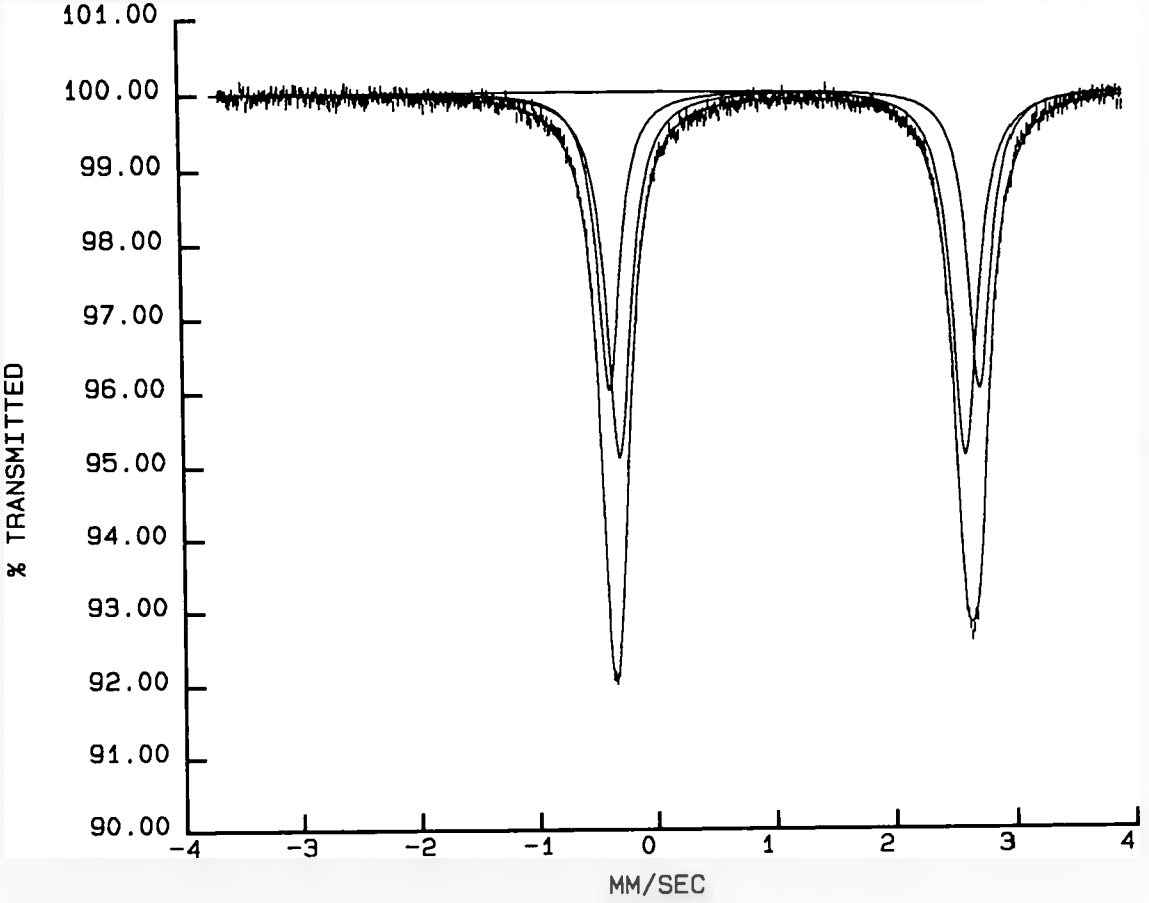

Figure 15. Mössbauer spectrum of olivine in Ep-3-139 D.

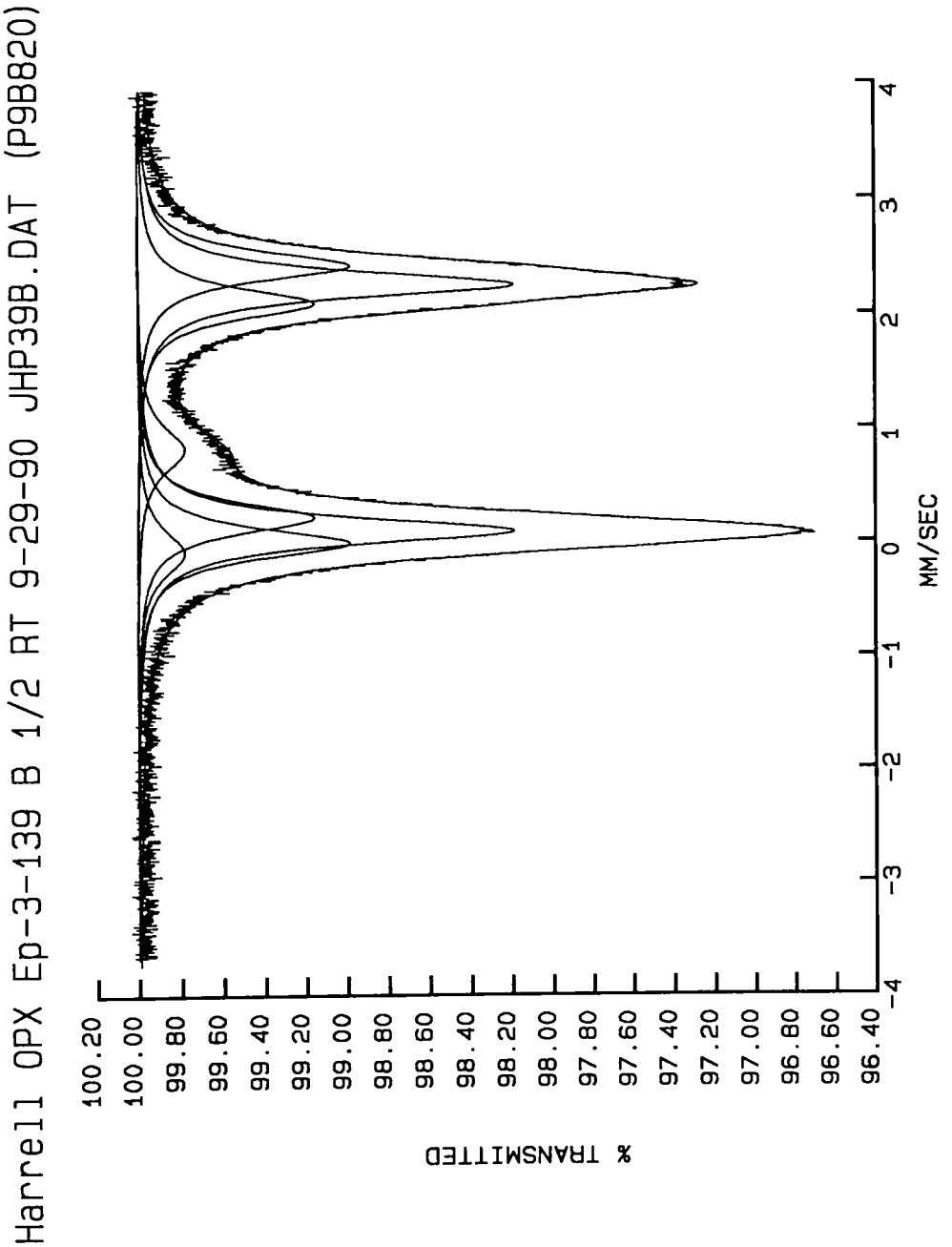

Figure 16. Mössbauer spectrum of orthopyroxene in Ep-3-139 B.

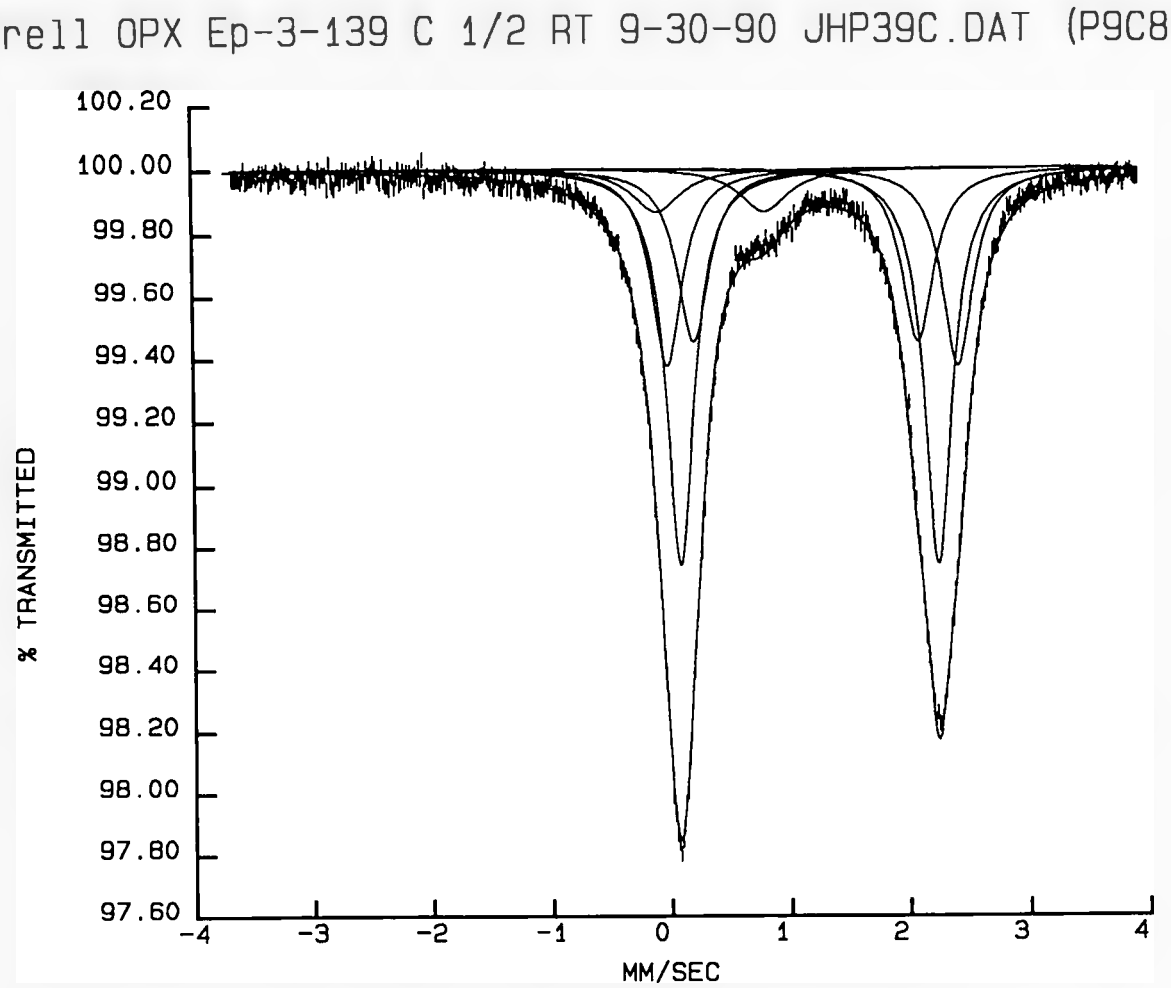

Figure 17. Mössbauer spectrum of orthopyroxene in Ep-3-139 C.

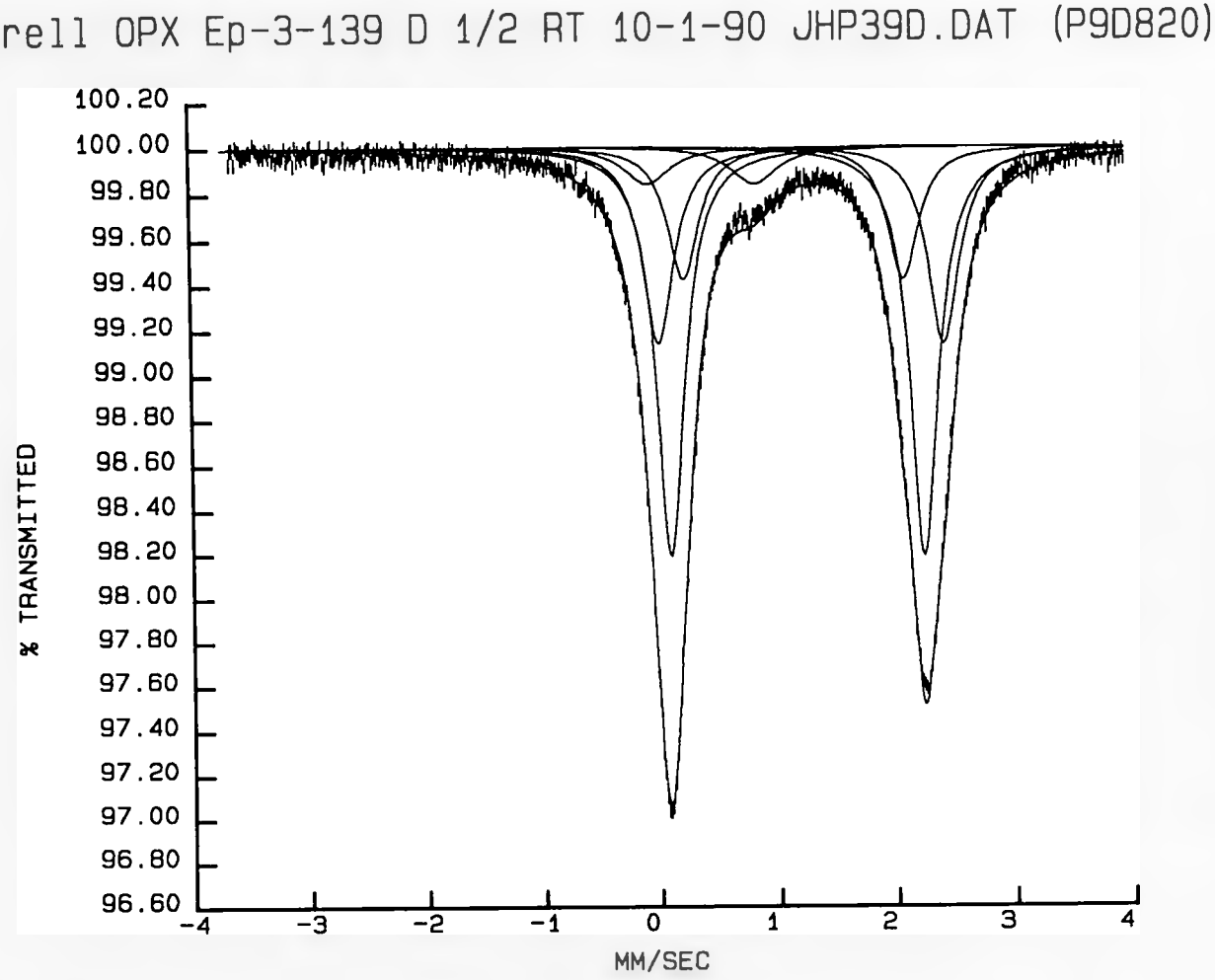

Figure 18. Mössbauer spectrum of orthopyroxene in Ep-3-139 D.

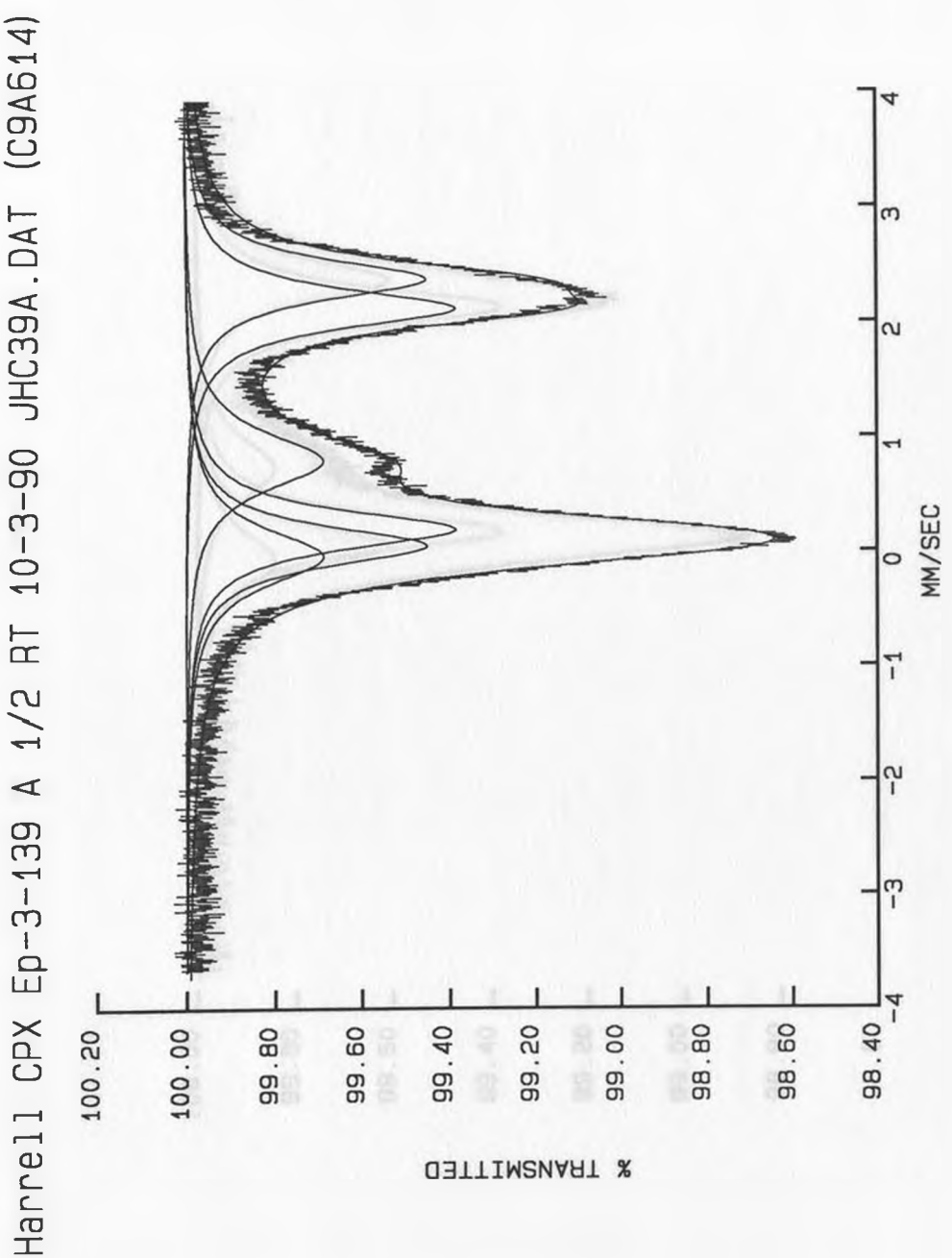

Figure 19. Mössbauer spectrum of clinopyroxene in Ep-3-139 A.

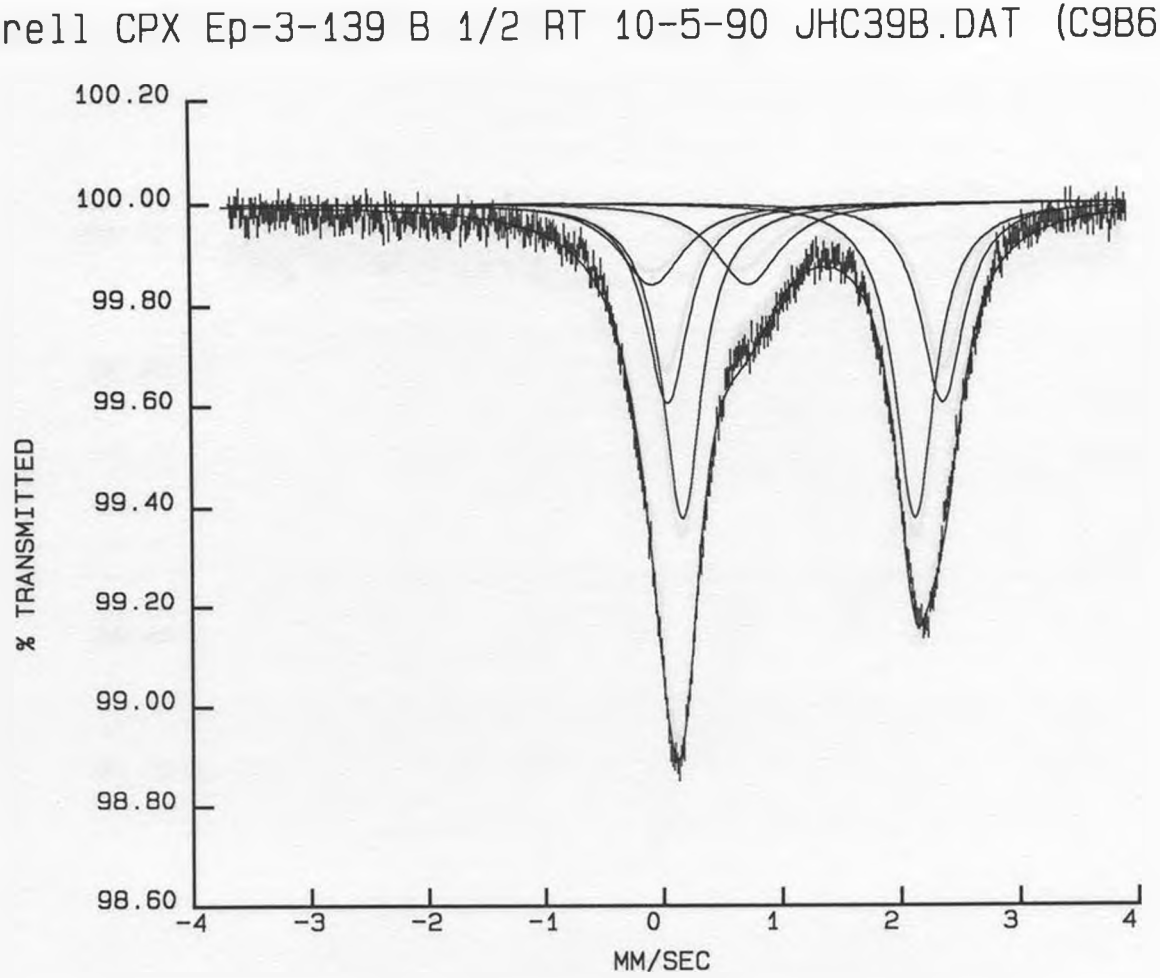

Figure 20. Mössbauer spectrum of clinopyroxene in Ep-3-139 B.

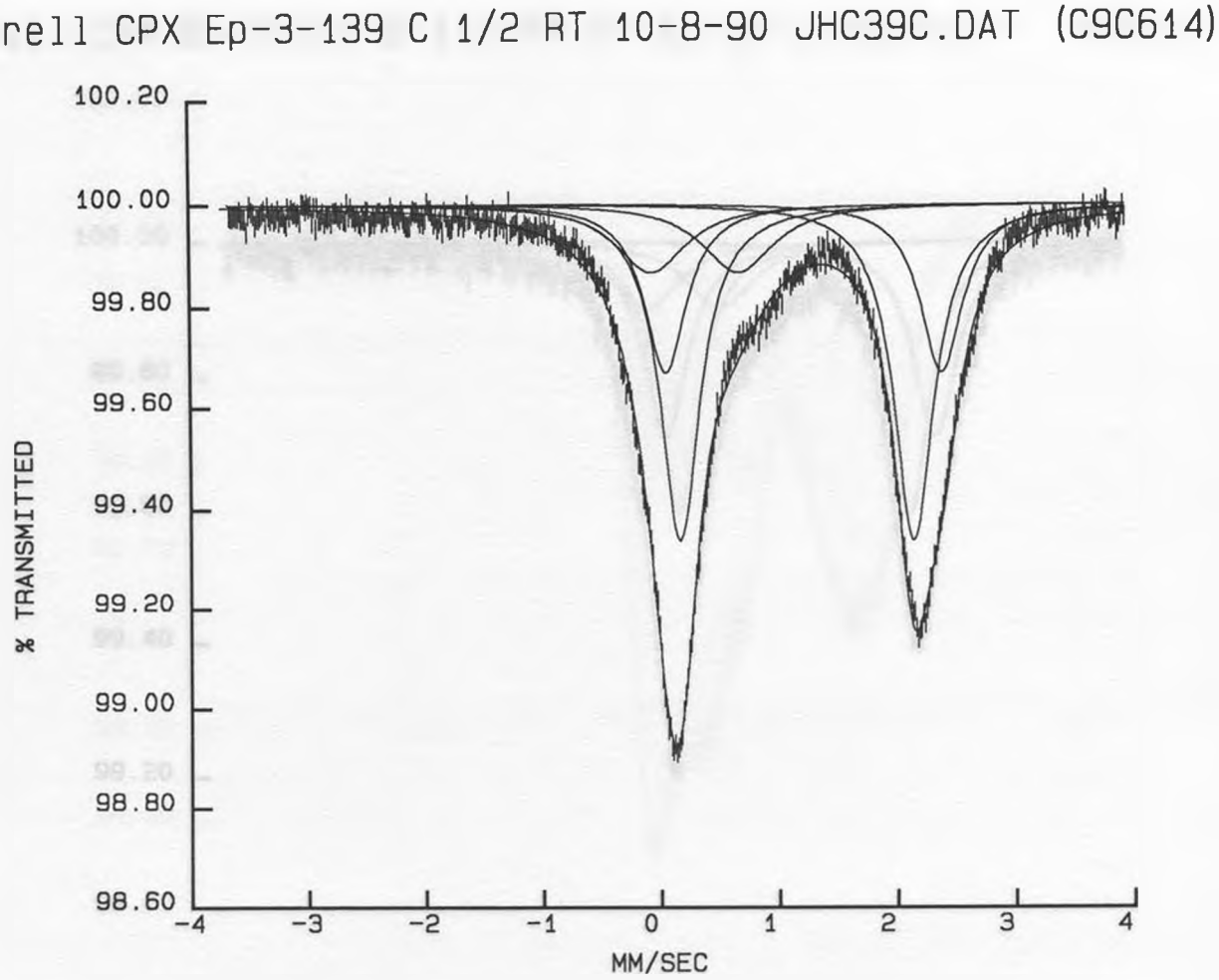

Figure 21. Mössbauer spectrum of clinopyroxene in Ep-3-139 C.

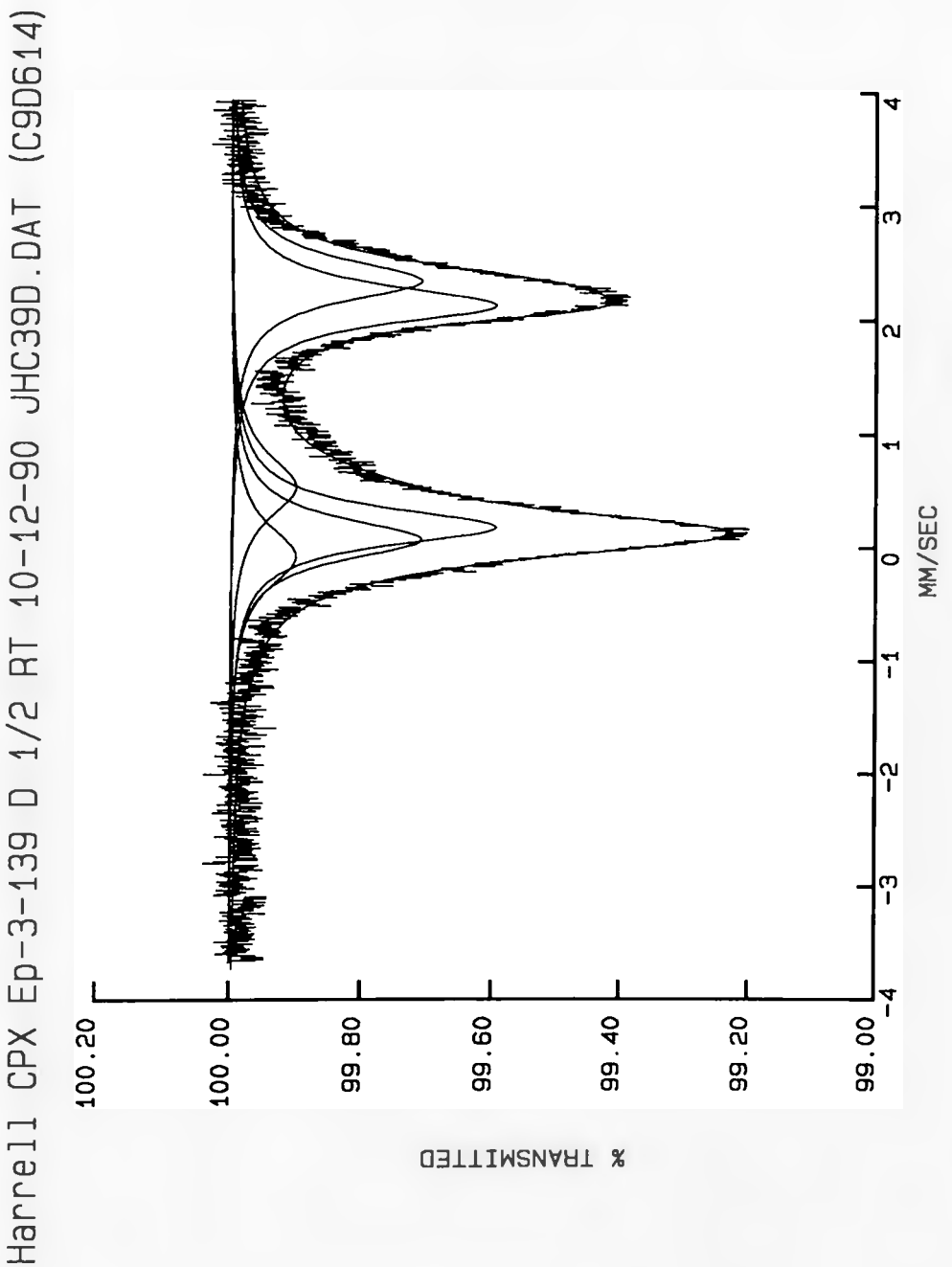

Figure 22. Mössbauer spectrum of clinopyroxene in Ep-3-139 D.

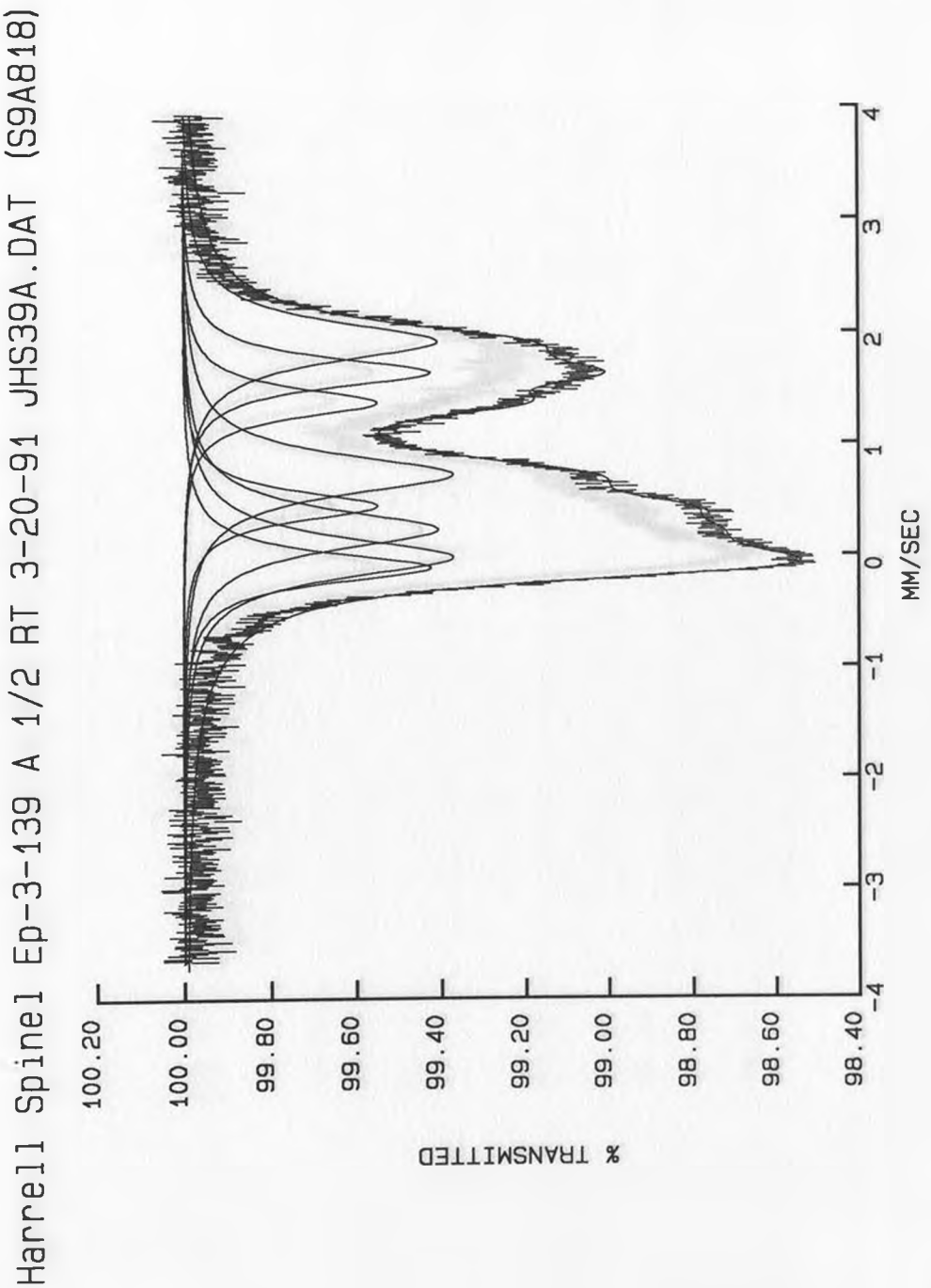

Figure 23. Mössbauer spectrum of spinel in Ep-3-139 A.

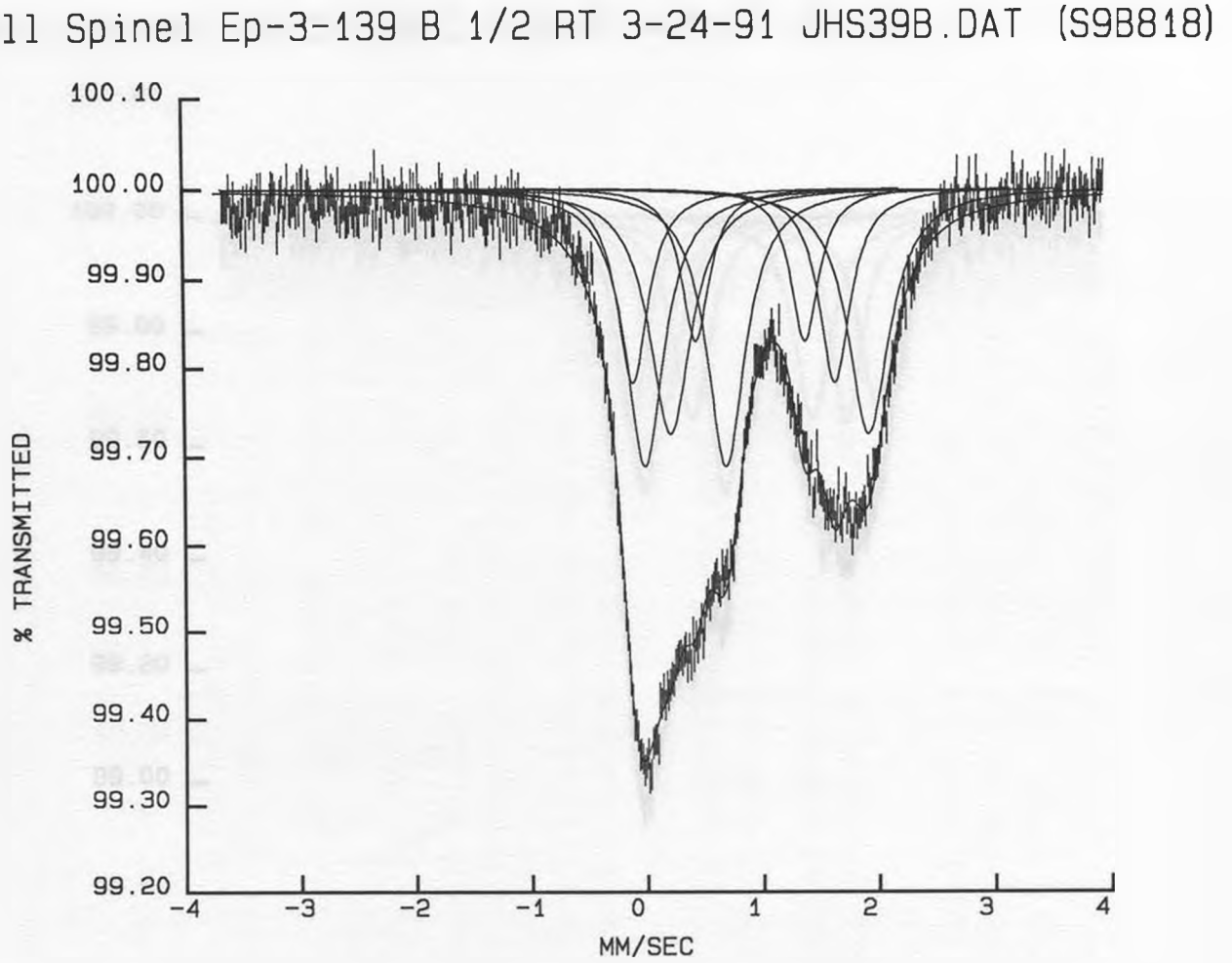

Figure 24. Mössbauer spectrum of spinel in Ep-3-139 B.

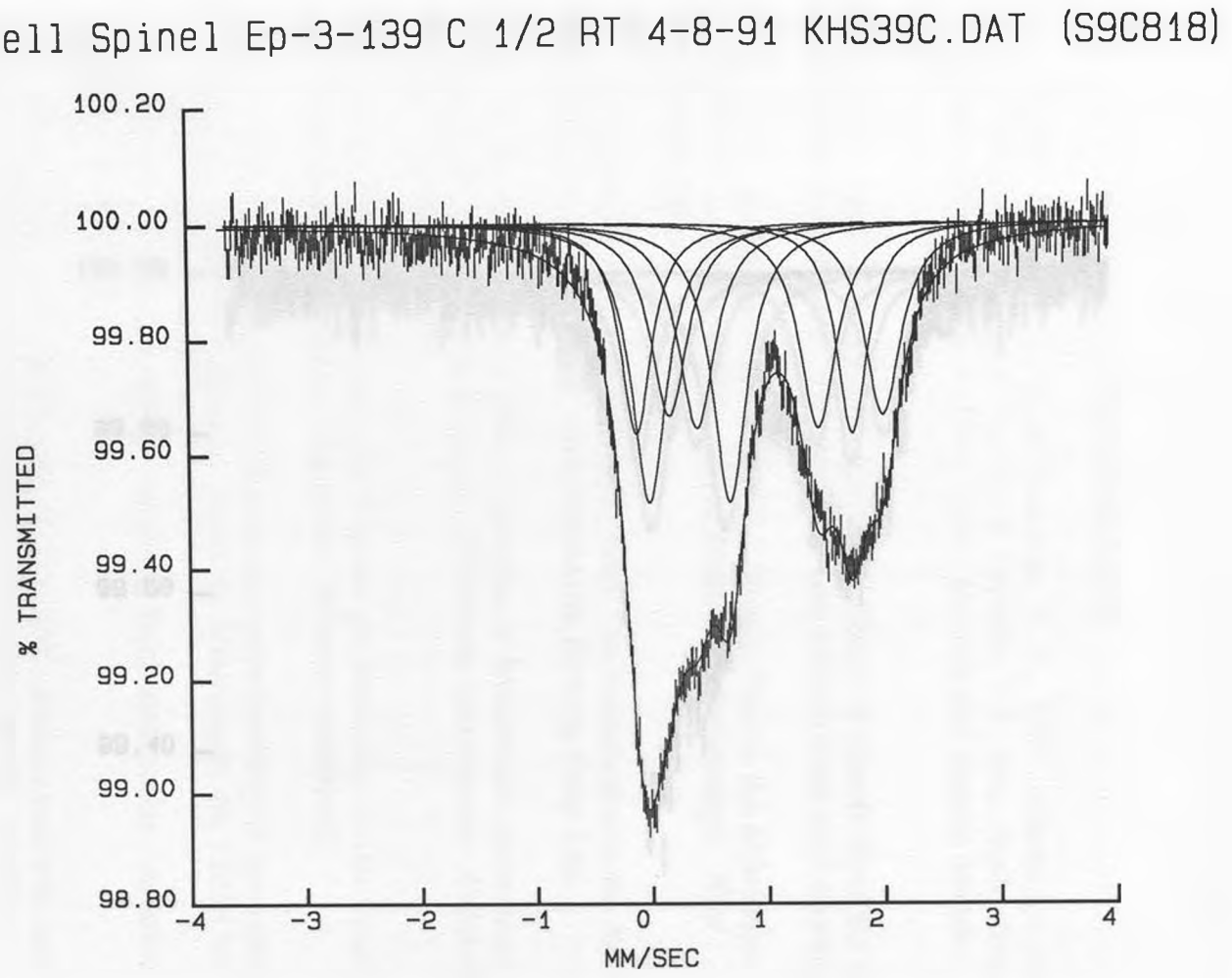

Figure 25. Mössbauer spectrum of spinel in Ep-3-139 C.

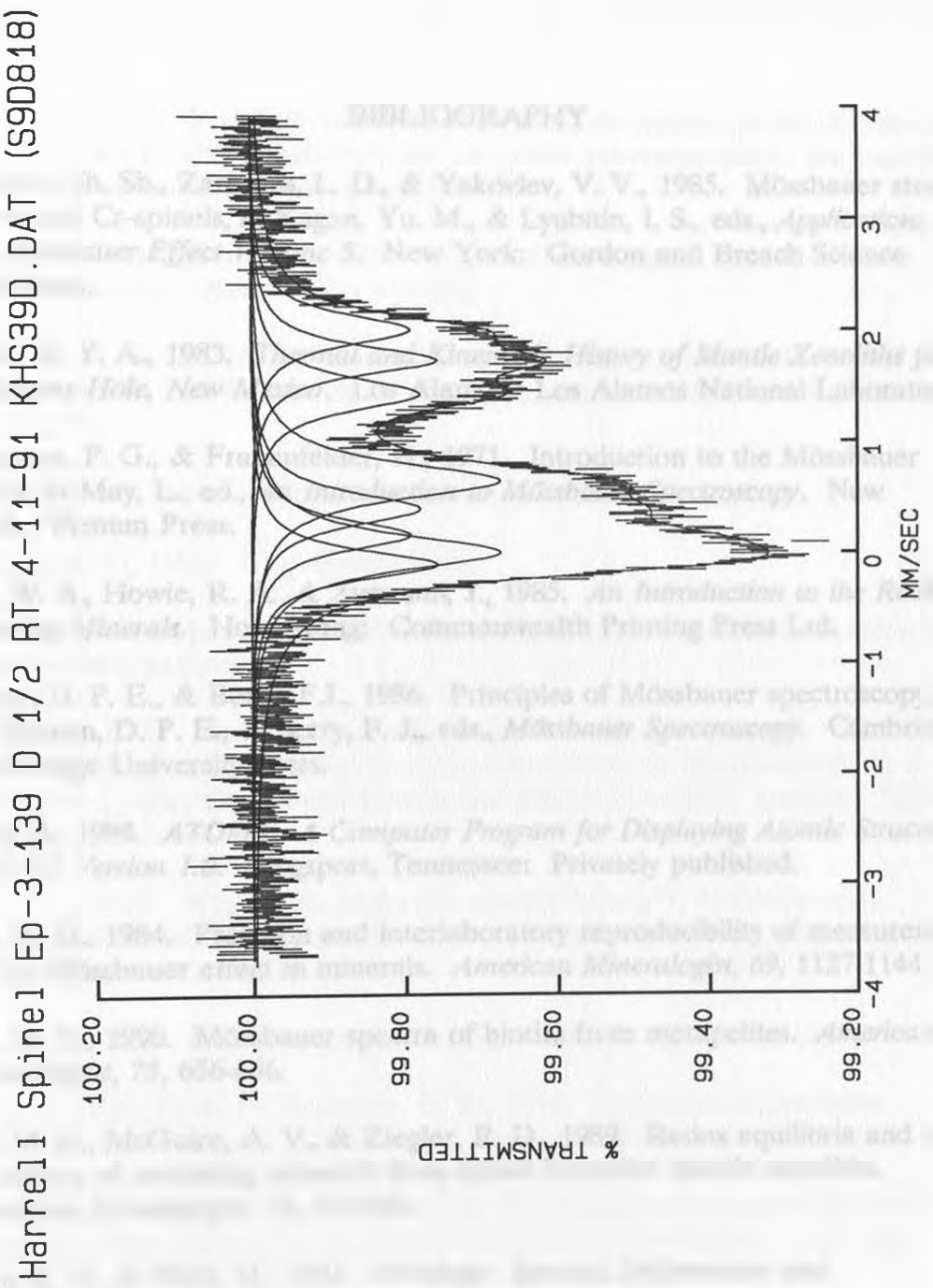

Figure 26. Mössbauer spectrum of spinel in Ep-3-139 D.

BIBLIOGRAPHY

Bashkirov, Sh. Sh., Zaripova, L. D., & Yakovlev, V. V., 1985. Mössbauer studies of natural Cr-spinels, *in* Kagan, Yu. M., & Lyubitin, I. S., eds., *Applications of the Mössbauer Effect Volume 5*. New York: Gordon and Breach Science Publishers.

Bussod, G. Y. A., 1983. *Thermal and Kinematic History of Mantle Xenoliths from Kilbourne Hole, New Mexico*. Los Alamos: Los Alamos National Laboratory.

Debrunner, P. G., & Frauenfelder, H., 1971. Introduction to the Mössbauer effect, *in* May, L., ed., *An Introduction to Mössbauer Spectroscopy*. New York: Plenum Press.

Deer, W. A., Howie, R. A., & Zussman, J., 1985. *An Introduction to the Rock Forming Minerals*. Hong Kong: Commonwealth Printing Press Ltd.

Dickson, D. P. E., & Berry, F.J., 1986. Principles of Mössbauer spectroscopy, *in* Dickson, D. P. E., & Berry, F. J., eds., *Mössbauer Spectroscopy*. Cambridge: Cambridge University Press.

Dowty, E., 1989. *ATOMS: A Computer Program for Displaying Atomic Structures, IBM-PC Version 1.0*. Kingsport, Tennessee: Privately published.

Dyar, M. D., 1984. Precision and interlaboratory reproducibility of measurements of the Mössbauer effect in minerals. *American Mineralogist, 69*, 1127-1144.

Dyar, M. D., 1990. Mössbauer spectra of biotite from metapelites. *American Mineralogist, 75*, 656-666.

Dyar, M. D., McGuire, A. V., & Ziegler, R. D., 1989. Redox equilibria and crystal chemistry of coexisting minerals from spinel lherzolite mantle xenoliths. *American Mineralogist, 74*, 969-980.

Ehlers, E. G., & Blatt, H., 1982. *Petrology: Igneous, Sedimentary and Metamorphic*. San Francisco: W. H. Freeman and Company.

Frey, F. A., & Prinz, M., 1978. Ultramafic inclusions from San Carlos, Arizona: petrologic and geochemical data bearing on their petrogenesis. *Earth and Planetary Science Letters, 38*, 129-176.

Hawthorne, F. C., 1988. Mössbauer spectroscopy, *in* Hawthorne, F. C., ed., *Spectroscopic Methods in Mineralogy and Geology, Reviews in Mineralogy, 18.* Washington: Mineralogical Society of America.

Irving, A. J., 1980. Petrology and geochemistry of composite ultramafic xenoliths in alkalic basalts and implications for magmatic processes within the mantle. *American Journal of Science, 280-A*, 389-426.

Mattioli, G. S., & Wood, B. J., 1986. Upper mantle oxygen fugacity recorded by spinel lherzolites. *Nature, 322*, 626-628.

Mattioli, G. S., Baker, M. B., Rutter, M. J., & Stolper, E. M., 1989. Upper mantle oxygen fugacity and its relationship to metasomatism. *The Journal of Geology, 97*, 521-536.

McGuire, A. V., 1990. Personal communication, June 26, 1990.

McGuire, A. V., 1991. Unpublished data.

McGuire, A. V., Dyar, M. D., & Nielson, J. E., in press. Metasomatic oxidation of upper mantle peridotite.

Menzies, M., 1983. Mantle ultramafic xenoliths in alkaline magmas: evidence for mantle heterogeneity modified by magmatic activity, *in* Hawkesworth, C. J., & Norry, M. J., eds., *Continental Basalts and Mantle Xenoliths*. London: Shiva Publishing Limited.

Ruby, S. L., 1973. Why Misfit when you already have χ^2?, *in* Gruverman, I. J., Seidel, C. W., & Dieterly, D. K., eds., *Mössbauer Effect Methodology, 9*. New York: Plenum Press.

Selby, M. J., 1985. *Earth's Changing Surface*. Oxford: Clarendon Press.

Skogby, H., Bell, D. R., & Rossman, G. R., 1990. Hydroxide in pyroxene: variations in the natural environment. *American Mineralogist, 75*, 764-774.

Stevens, J. G., 1981a. Useful equations for Mössbauer spectroscopy, *in* Robinson, J. W., ed., *Handbook of Spectroscopy, III*. Boca Raton, Florida: Chemical Rubber Company.

Stevens, J. G., 1981b. Useful constants, *in* Robinson, J. W., ed., *Handbook of Spectroscopy, III*. Boca Raton, Florida: Chemical Rubber Company.

Stone, A. J., Parkin, K. A., & Dyar, M. D., 1984. STONE: A curve-fitting program for Mössbauer spectra. *DEC User's Society Publication, 11-720.* Marlboro, Massachusetts.

Streckeisen, A., 1976. To each plutonic rock its proper name. *Earth Science Review, 12,* 1-33.

Wilshire, H. G., Meyer, C. E., Nakata, J. K., Calk, L. C., Shervais, J. W., Nielson, J. E., & Schwarzman, E. C., 1988. *Mafic and Ultramafic xenoliths from Volcanic Rocks of the Western United States.* Washington: United States Government Printing Office.